CHARACTERIZING THE OPTICAL PROPERTY OF PLAMONIC NANOMATERIAL AND USE THEM TO DEVELOP A TOOL FOR WASTEWATER TREATMENT

By

MD Faqrul Islam

16321142

Mehzabien Iqbal

16121048

Tasin Rahman

19121151

Abu Yousha Mohammad Abdullah

16121138

A thesis submitted to the Department of Electrical and Electronic Engineering in partial fulfillment of the requirements for the degree of
Bachelor of Science in Electrical and Electronic Engineering

Electrical and Electronic Engineering
Brac University
December 2019

Declaration

It is hereby declared that

1. The thesis submitted is my/our own original work while completing degree at Brac University.
2. The thesis does not contain material previously published or written by a third party, except where this is appropriately cited through full and accurate referencing.
3. The thesis does not contain material which has been accepted, or submitted, for any other degree or diploma at a university or other institution.
4. I/We have acknowledged all main sources of help.

Student's Full Name & Signature:

MD Faqrul Islam 16321142	**Mehzabien Iqbal** 16121048
Tasin Rahman 19121151	**Abu Yousha Mohammad Abdullah** 16121138

Approval

The thesis/project titled "Characterizing the optical property of plasmonic nanomaterial and use them to develop a tool for wastewater treatment" submitted by

1. MD Faqrul Islam (16321142)
2. Mehzabien Iqbal (16121048)
3. Tasin Rahman (19121151)
4. Abu Yousha Mohammad Abdullah (16121138)

of Fall, 2019 has been accepted as satisfactory in partial fulfillment of the requirement for the degree of Bachelor of Science in Electrical and Electronic Engineering on 24th of December.

Examining Committee:

Supervisor:
(Member)

_____
Abu S.M. Mohsin, PhD
Assistant Professor, Department of Electrical and Electronic Engineering
Brac University

Program Coordinator:
(Member)

_____
Abu S.M. Mohsin, PhD
Assistant Professor, Department of Electrical and Electronic Engineering
Brac University

Departmental Head:
(Chair)

_____
Shahidul Islam Khan, PhD
Professor and Chairperson, Department of Electrical and Electronic Engineering
Brac University

Abstract/Executive Summary

Water pollution is one of the vital problems in Bangladesh. This problem is increasing with the huge number of population and implementation of proper management system. Our thesis work is mainly focused on water purification in order to use it in our daily activities. For this purpose, we choose nanoparticle to refine water. To do so, we did a systematic analysis to characterize the silver and gold nanoparticle by using Finite Difference Time Domain (FDTD) (lumerical solution Inc.) simulation for numerical analysis and Mie theory for analytical analysis. Further, we did some experiments to identify different types of bonding, presence of elements and their quantity, pH level in wastewater sample, which was collected from different sources. This paper shows some graphical analysis to observe the scattering, absorption and extinction characteristics of nanoparticle, demonstrates the technique to identify the presence of nanoparticle in wastewater sample through extensive simulations and rigorous experiments. Our tool is not only for characterization of nanoparticle but also identify the harmful molecules that are present in our sample, which leads to remove those molecules in future. To conclude, we have developed a technique that not only identifies the existence of nanoparticles in wastewater, but can also be used to refine wastewater and reuse wastewater.

Dedication

DEDICATED TO OUR PARENTS AND OUR SUPERVISOR, DR. ABU S.M. MOHSIN, WHO WORKED DAY AND NIGHT, TO HELP US REACH THE POSITION WE ARE NOW IN.

Acknowledgement

At first, we would like to convey our best gratitude to almighty Allah for His kindness and blessing. Without His will it would not have been possible for us to finish this thesis paper which we consider to be our one of the most important learning experiences of our undergraduate life.

We are forever indebted to our supervisor Dr. Abu S.M. Mohsin, Assistant Professor, Department of Electrical and Electronic Engineering, Brac University, for providing us with an extraordinary opportunity to work in the arena of nanophotonic and nanotechnology. We consider ourselves very lucky to have got his tireless support and inspiring guidance during the period of research. Next, we would like to express our heartfelt appreciation to all the faculties and staffs of Electrical and Electronic Engineering Department of Brac University for their unconditional assistance in our hours of need.

At last we would like to thank our parents for always standing by us. It is their care, support and sacrifice that has encouraged us to come this far. We are very much thankful for everything they have done for us.

Table of Contents

List of Tables

List of Figures

List of Acronyms

NPs	Nanoparticles
DNA	Deoxyribonucleic acid
EBL	Electron Beam Lithography
FIB	Focused Ions Beam
NIL	Nanoimprinting Lithography
SPR	Surface Plasmon Resonance
LSPR	Localized Surface Plasmon Resonance
FDTD	Finite Difference Time Domain
GDM	Green Dyadic Method
DDA	Discrete Dipole Approximation
FTIR	Fourier Transform Infrared Spectroscopy
AAS	Atomic Absorption Spectroscopy
XRD	X-Ray Diffraction
FESEM	Field Emission Scanning Electron Microscopy

Chapter 1

Introduction

1.1. Introduction to Plasmonic Nanoparticles

Plasmonic nanoparticles refer to particles whose electron density interact with electromagnetic wavelength radiation, leading to delocalization of electron cloud. This results to rise of new types of material properties which are previously unavailable in the particle. The wavelength of electromagnetic material is generally far greater than the particle due to its tendency of being dielectric-metal interface between the medium and the particles: unlike in a pure metal[1].

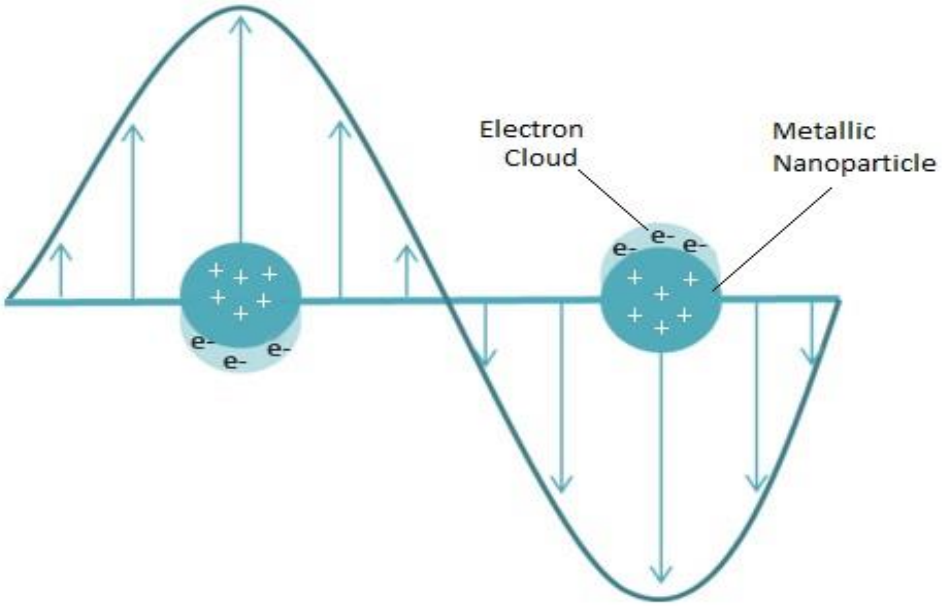

Figure-1.1: Oscillation of plasmonic material

What separates these particles from ordinary surface plasmons is that the plasmonic nanoparticles additionally expresses unique properties absorbance, and coupling, depending on their geometries and relative positions[2,3]. These unique traits have made them important in the field of application of solar cells, spectroscopy, signal enhancement for imaging, and

cancer treatment[2,4]. They are a good choice for designing mechano-optical instrumentation due to their high sensitivity[4].

1.2 Applications of Plasmonic Nanoparticles

Nanoparticle has rapidly gained its publicity worldwide for its multiple opportunities in usage for practical applications. Metal nanoparticles such gold and silver, possess various optical properties which can be used to solve various problems of our daily lives. Many medical processes such as treating cancers, involves the use of nano-probes as heaters to kill cancerous cells. Furthermore, nanoparticles play vital roles in providing renewable green energy to our environment. Photovoltaic devices have increased efficiency and effectivity due to the usage of plasmonic nanostructures[5]. In this section, various applications of nanomaterials have been identified and discussed thoroughly.

1.2.1. Plasmonic nanoparticle in Water Treatment

Heavy Metal Removal

Metal nanoparticles plays a huge role as adsorbents in water purification. They have a large surface area which allows them work well as sorbents. Additionally, they can be treated with various chemicals in order increase their affinity towards substances that need to be removed from waste water.

Using Iron oxides

Iron is one of the most readily available metal on earth. High availability and ease of production makes nanosized ferric oxides (FeO) to be low-cost adsorbents for toxic metal sorption such as copper. They can be directly pumped into contaminated areas due to its environmental-friendly nature, for maximum effect. Goethite (FeOOH) can be prepared from $Fe(NO_3)_3$ precipitation[6, 7]. They have a needle-like structure, with length of 200nm and a surface area of 50 m^2/g. Such a large surface area allows 100% removal of Cu^{2+} at an adsorption rate of $10^{6.81}$L $mol^{-1}s^{-1}$ and desorption rate of $10^{4.88}$L $mol^{-1}s^{-1}$[7]. Hematite (Fe_2O_3) are of granular in shape, with a crystal size of 75nm, shows a rate of removal of around 149.25mg/g of Cu[6, 8]. Nano-maghemite (FeO_3)has shown high affinity for Cr(VI) removal from water. The adsorption capacity of nano-maghemite for Cr (VI) (19.2 mg/g) is much greater than diatomite (11.55 mg/g)[9], anatase (14.56 mg/g)[10], commercial activated

carbon (15.47 mg/g), and beech sawdust (16.13 mg/g), which were previously used for removal of Cr (VI)[6, 11].

Using Hydrous Manganese Oxide

Pb (II), Cd (II), and Zn (II) undergo adsorption onto Hydrous Manganese Oxide by ionic exchange, forming inner-sphere complex formation. There is a rapid adsorption of metal ions to the external surface of Hydrous Manganese Oxide, consequently resulting to a slow intra-particle diffusion along the micropore walls[12]. Furthermore, mixed-valence manganese oxides with 3 to 6 layers and 7 to 11 tunnel structures are also considered as good sorbents for cations of Strontium (^{89}Sr) and Cesium (^{137}Cs). And for separation of trace silver ions. Their good selectivity coefficient and high exchange rate for ion allows them to be good used properly for various water cleaning purposes.

Using Nanosized Titanium Oxide

TiO_2 anatase, a form of TiO_2, is used in various industrial applications of metal removal. TiO2 nanoparticles are well known for the successful removal of metallic particles, in the presence of UV light and adsorption, from water[13]. TiO_2 anatase, (with surface area of 185.5 m2/g and 9.5 m2/g for bulk particles, and a value of pH_{pzc}= 5.2 [6, 13]) were able to simultaneously remove multiple metals (Zn, Cd, Pb, Ni, Cu) from a solution of pH = 8 and a San Antonio tap water. In another study[14], nano- TiO_2 (BET surface area of 208 m2/g, diameter of 10 to 50 nm) showed adsorption rate of Zn and Cd to 15.3 and 7.9 mg/g, respectively, at a pH value of 9.0[6]. The availability of other forms of ions (100–5000 mg/L) has no significant effect on the focused metal (Zn2+ and Cd2+ ions of 1.0 mg/mL) adsorption under these specific conditions.

Antibacterial Nanoparticle

Dendrimers

Dendrimers are macromolecules with spherical and symmetrical structure, consisting of a dense compact shell. It has a definite surface which is a result of its composed of a core-branching sites and terminal groups[15, 16]. Dendritic polymers show numerous features that make them especially appealing as useful materials for water sanitization. These 'delicate' nanoparticles, with sizes of 1 to 20 nm, can be utilized as strong recyclable water solvent

ligands for radionuclide, inorganic anions and noxious metal particles[16, 17].Dendritic polymers can likewise be utilized as platforms or templates for the catalytical active nanoparticle preparation or as recyclable unimolecular micelles for recouping natural solutes from water[16, 18].

Antimicrobial agents such as Ag (I) and quaternary ammonium chlorides are known to use dendritic macromolecules (i.e. PANAM) as a transferring agent in various water treatment processes. Due to the nuclear/atomic level scattering of the visitor in a dendrimer host, the activity remains grasped if the microorganism can establish contact with the nanocontainers; silver domain. Perceptibly, the silver ions remain adjoined to the dendrimer, forming cluster or compounds. Diffusion takes place, transferring the silver present in the agar medium, via soluble dendrimers host[16]. Since the dendrimer have is solvent, it is ready to convey the immobilized silver in the agar medium by its own dispersion. The silver clusters remain active due to their large surface area.

Silver Nanoparticles

The incorporation of silver nanoparticles into a range of low-cost materials as an antibacterial water filter treatment is a relatively new solution to drinking-water problems. Silver nano-particles consist of high surface-area-to-volume ratio. This results in a broad and strong spectrum for antimicrobial activities in drinking water.

During polymerase chain reactions, silver ions enhance DNA mutation, preventing the bacteria to grow and replicate. They can act also as catalysts to produce reactive organic species (**ROS**) in the presence of dissolved oxygen. They speed the chemical reactions with oxygen, resulting in the formation of free radical from the surface of the silver nanoparticles and inducing bacterial membrane's damage[19, 20]. In other studies[20, 21], it showed that AgNP demilitarize bacteria by attaching to its cell membrane and prohibiting microbial growth. Penetrating inside the membrane cell wall, they damage the bacterial cell, increasing permeability, thus disrupting its process of respiration and damage fundamental functions, such as maintaining enzyme signal activity, respiratory processes, as well as the cell oxidation[22]. The DNA molecules become condensed and lose their capability to replicate, leading to their inactivity[23]. Further analysis shows[24, 25], there has been an establishment of electrostatic force of attraction between a negatively charged bacterial cell surface Escherichia coli (E. coli), and a positively charged material (AgNP), which increases the this removal process by great length.

Membrane and Water Treatment

Nanostructured catalytic membrane is a type of membrane that is utilized mostly for treatment of tainted water. It consists of institutionalized catalytic sites, which participates in different process of water treatment, producing clean water for all. The membrane breaks down organic pollutants, isolating the contaminants physically. To remove harmful substances from water, membranes doped with N-dope nanomaterials, are highly efficient due to their process of enhancing photo degradation activity. Studies revealed that clean water can be produced with high fluctuations, with a scale level of 20-400 nm for the nanostructured films and membrane[15, 26].

Biomimetic membranes are also involved cleaning process of waste water. The principle of reverse Osmosis plays a vital role in such procedures. Biomimetic membranes clean out salt and other harmful substances from the water and make it suitable for various uses[15].

Another such useful membrane is Ceramic Membrane. Ceramic membrane is widely known for its longevity, thermal and chemical stability. It ensures high level of stability in mechanical purposes and biological inertness creates detrimental effect on wastes, available in water. They are highly porous, with small pore size distribution. These types of membranes are developed by vapor gatherings in the pores of borosilicate Pyrex membranes, synthesized from Carbon nanotubes and are effective in removal of aerosol and bioaerosol from water. The pores are micrometer in size and are used to capture leached out metallic nanoparticles[15, 27, 28]. Silver and copper nanoparticles are used as catalysts to grow carbon nanotube fiber over activated carbon fibers, which makes it effective against bacteria like staphylococcus aureus. Thus, efficiency and cost are easily maintained by the use of membranes

Removal of Organic Dye Solvent

Color is the first contamination that can be clearly recognized on wastewater. Dyes are used in industries for various purposes, resulting in a considerable amount of colored substance on wastewater. The presence of these dye, even at very scarce concentration is health-hazardous and undesirable. The degradation by-products of organic dyes such as synthetic azo-dyes

have severe consequences on the environment since they contain toxic aromatic amine compounds and the removal rate of these materials during aerobic waste treatment are still low. Nowadays, plasmonic NPs are of great use for the efficient removal of these dyes.
Maghemite (Fe_2O_3suspension) consist of hydroxyl groups, with various pH value, enclosed to the surface of the metal. The surface at pH_{zpc} (the pH of zero-point charge) has a neutral charge, while pH_{zpc} of maghemite nanoparticles is around 6.3 [29, 30]. Below this value of pH_{zpc}, the adsorbent surface has a positive charge, and resulting in adsorption of anion. As the CR solution's pH is increased, there is a relative decrease in adsorption due to the progressive deprotonation of hydroxyl branch on the adsorbent and electrostatic repulsion between negatively charged sites on the adsorbent and color anions[30]. Furthermore, the metal surface of maghemite can absorb CR ions at a greater rate by the coordination effect between metal ions and amine groups at the ends of CR molecules[31]. Thus, it can be concluded that metal oxides with the higher surface area can adsorb more CR molecules.

TiO_2 can also remove azo dyes from wastewater, using photocatalytic oxidation In the photocatalytic oxidation, TiO_2 has to be exposed and excited under UV light to induce charge separation[32]. On contrast, dyes rather than $TiO_2$are excited by visible light followed by electron infusion onto the TiO_2 conduction band, which leads to photosensitized oxidation. Subsequently, this is followed by electron injection from the energized dye molecule onto the conduction band of the TiO2 particles, whereas the dye is transformed to the cationic dye radicals (Dye·+) that undergo degradation to yield products, which can safely be removed[32].

1.2.2. Plasmonic nanoparticle in biological application

Plasmonic nanoparticles (PNPs) have unique size, shape, orientation and tip geometry which produces astounding optical properties, such as absorption, scattering, tunability, etc in the visible to near infrared regions. They are known to be highly durable due to its anti-bleaching effect which makes them good component for biological cell applications, such as bio-labelling and sensing, biological imaging, photothermal cancer therapy, probing membrane protein and drug or gene delivery[33] .

Recently, nanoparticle plasmon coupling are being used to investigate the interparticle distance between two micro molecules using plasmon ruler, by using the analogy of spectral shift due to coupling of two gold nanospheres (AuNS). This process is effective in probing membrane proteins on cell surface receptors, to follow receptor trafficking and to detect aggregation of PNPs inside cells through receptor trafficking[33].

Plasmonic nanoparticles is well known for light scattering and reflection. So, they can be easily identified under dull field enlightenment and by other methods [34, 35]. Thus, they are having better results compared to commonly used organic fluorescent dyes, when used in vitro biological applications, for the study of nanoparticle–cell interactions, disintegration during imaging, or exhibiting photobleaching [36]. In contrast, plasmonic nanoparticles are photo stable and thus can be used as bio-nanoprobes to control consecutive various events over a period of time with a stable signal. For instance, gold nanoparticles biofunctionalized with epidermal growth factor (EGF) on their surface have been selectively attached on cancer cells. These cells overexpress the epidermal growth factor receptor (EGFR) on their surface, thus the gold nanoparticles selectively attach on them as verified by dark field microscopy [37, 38]. Therefore, such plasmonic nanoparticles can be employed as advanced bio-nanoimaging agents that are used by biologists to monitor specific drug effects on cells or to identify specific pathways.

Magnetic nanoparticles also lead a vital role in bio-applications. They are highly implemented in magnetic resonance imaging contrast agents, and can also be used in arranging or isolating magnetic cells. Normally, iron oxide nanoparticles are considered as they are superparamagnetic, and therefore, exhibit the display ideal attractive properties within the range of magnetic field. Furthermore, iron oxide can also be used as therapeutic agents by hyperthermia Therefore, consolidating them with plasmonic nanoparticles open up new doors to multimodal imaging and treatment.

1.2.3 Plasmonic nanoparticle in sensing (sensors)

Carbon nanomaterials are frequently used as sensing elements. Carbon nanomaterials-based sensors usually have high sensitivities and lower detection limits than their other types of sensors[39-41]. They provide a stable activity in the structure of proficient electrochemical sensors; all of which increases their efficiency of electron transport kinetics. Biosensors made

from carbon nanotubes gives a clear identification of biomolecules for in vivo and in vitro applications[41, 42]. Carbon nano horns and carbon nanofibers are newly invented nanomaterials which have been explored as novel and biocompatible matrices for the design of devices related to biosensing[41, 43]. Conductive mesocellular silica–carbon nanocomposite foams are providing unique and effective results related to protein biosensing and immobilization[41, 44]. Stable and sensitive reagent less sensor for hydrogen peroxide are recently being constructed using Single-walled carbon nano horns[45]. The doping of carbon nanostructures with nitrogen atoms created a huge impact in the world of science. Nitrogen doped carbon nanotubes have various applications and uses in the production of sensors for the detection of glucose [46, 47]. Electrochemical biosensors that attaches enzymes into nanomaterials provide novel constructs with synergistic properties that develops from the constituents of hybrid compositions. Graphene, as a genuine two-dimensional material, has gotten expanding considerations due to its exclusive physicochemical properties and has attracted considerable scientific and technological interest in past few years[41].

Gold and silver nanoparticles are used as plasmonic biosensors for identification of specific biomolecules and proteins ions that are related to specific diseases. The plasmon extinction (absorption and scattering) band of such nanostructures depends on the refractive index of the medium surrounding them. A higher refractive index means it causes a red-shift. The refractive index of proteins or DNA is greater than that of buffer solutions, therefore, upon attachment on the plasmonic surface, the local refractive index increases. This causes the plasmon extinction band to shift to higher wavelengths, which is termed the biosensor response[48].

1.2.4 Plasmonic nanoantenna

A nanoantenna is a solar oriented assortment gadget dependent on rectified antennas. It comprises of three primary parts: the ground plane, the optical resonance cavity and the antenna. The nano-antenna consumes electromagnetic wave, the ground plane acts to mirror the light back towards the antenna and the optical resonance cavity reflect and concentrates the light back towards the antenna by means of the ground plane.

One of the major advantages of nano-antenna is its high theoretical efficiency. For instance, the theoretical efficiency of a single solar cell is only 30%[49]. In contrast, nanoantenna the theoretical efficiency found is nearly 85%[49]. Another advantage of nanoantenna over semiconductor photovoltaic devices is that nanoantenna arrays can be designed to ingest any frequency of light[49]. Nanoantenna can absorb energy from sunlight as well as the earth's heat emitted in the form of infrared radiations.

The theory behind nanoantenna is essentially the same for rectifying antennas. Light incidence on the antenna causes the electrons in the antenna to move back and forth continuously at a similar frequency as the incident light[49]. This is caused by the oscillation of electric field, present in the incoming electromagnetic wave. The movement of electrons produces an alternating current in the circuit of antenna. To convert this power into DC, the AC current is rectified, using various diodes. The resulting DC current can then be used to power any types of external load.

The fabrication of nanoantenna has been done using several techniques like Electron Beam Lithography (EBL), Focused Ion Beam lithography (FIB) and Nanoimprinting Lithography (NIL). Various types of nano-antennas are available nowadays. These includes Graphene Antennas, Carbon Nanotube Antennas, gold and silver nano-antennas.

1.3 Optical Properties of Plasmonic Nanoparticle

The comprehensive optical properties of plasmonic Nano structures is one of the most research topic in the field of Nano photonics. Optical properties refers to determine the better plasmonic material at specific wavelength by varying particle's structure[50]. SPR (Surface Plasmon Resonance), LSPR (Localized Surface Plasmon Resonance), Mie scattering, extinction and absorption, field enhancement, far field angular scattering and quantum yields include optical properties of plasmonic material [50-52].Optical properties have been evaluated based on refractive indices and dielectric function defined by Drude model and Mie theorem [51, 53]. The following section refers the optical properties to characterize plasmonic Nano material in various application.

1.3.1 Optical properties – Absorption, Scattering and Extinction

Absorption cross section is the capacity of a plasmonic Nano particle to absorb a photon of a specific polarization and wavelength. Scattering cross section occurs when Nano particle

absorb photon, they re-emit the energy of light with various intensity in different direction. Extinction cross section is a summation of scattering cross section and absorption cross section [51, 54, 55]. These, optical properties can be determined by using Mie and Rayleigh theory [51].Mie theory is an illustrative arrangement of Maxwell's equations for the scattering of electromagnetic radiation by particles of any measure (particularly sphere) [51, 54, 56, 57]. Mie theory is utilized broadly in electromagnetic simulations of spherical Nano particle and the properties of nanoparticle's LSPR are simulated by generalized Mie theory.

1.3.2 Optical properties – Field Enhancement

In a metallic-dielectric interface, surface plasmons (SPs) are excited for photons [58]. Plasmons have a very strong localization and electromagnetic field, since local field enhancement determines the ratio of the incident electrical field and local electrical field when an incident wave triggers or induces Nano plasmonic structure [59].For illustration, for Nano-plasmonic spherical structure – gold, silver is excited by an incident plane wave; optimum enhanced field can be measured when the real part of the dielectric function is ignited. Approximately through Mie scattering or numerical simulations including GDM (Green Dyadic Method), DDA (Discrete Dipole Approximation), and FDTD (Finite Difference Time Domain) can be found in their scattering cross sections and electromagnetic fields [58, 60, 61].In addition, by changing the structure of Nano material, field enhancement can increase. Nano spherical plasmonic coupling effect causes significant near-field improvement that is much larger than plasmon [61].

1.4 Aims and Methodology of the thesis

In this section, the specific aims of this thesis, potential research problems and proposed techniques to achieve the intended goals will be discussed.

The aim of this thesis is to characterize the nanomaterial and uses the plasmonic property to develop a tool for wastewater treatment. To do so, we divided our thesis into two parts; first part consisting of the characterization of the optical properties of plasmonic nanomaterials, while the second part deal with the identification of nanomaterials present in waste water, so that we can develop a tool in order to remove this materials and provide a much better source of clean water to the environment.

In order to achieve our aim, we use a clear methodology to reach our end results. We approached this methodology by developing analytical and numerical FDTD simulation for

study of silver and gold nano-particle. We also carried out experimental analysis which included Fluorescence spectroscopy, Atomic Absorption Spectroscopy, pH and Fourier

Transform Infrared Spectroscopy, in order to support our analysis done on the analytical part.

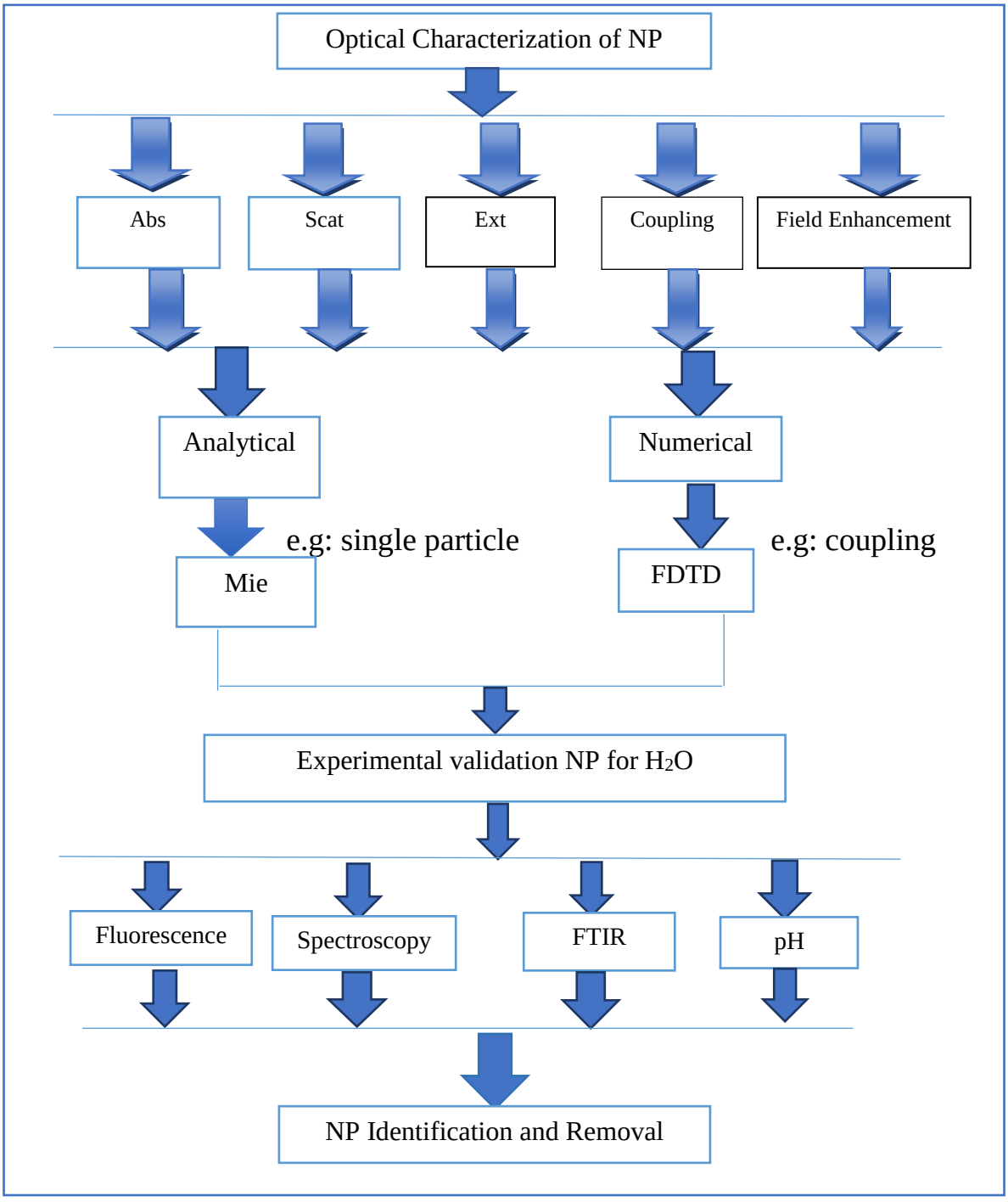

Figure-1.2: The flowchart of research study process – summary of our thesis analysis with relevant diagram

1.5 Thesis structure

The research of our thesis work has been categorized into numerous chapters. Each chapter principally focused on a particular part to achieve precisely the goals of our research analysis that is characterizing the nanomaterial and uses the plasmonic property to develop a tool for wastewater treatment. To begin with, the literature review of plasmonic nanoparticles and their application in the field of nanotechnology such as biological imaging cell application, sensor, nano antenna, plasmonic circuitry and wastewater management have been illustrated in our introductory chapter. Second, the established wastewater purification techniques using plasmonic nano material such as removal of heavy metals, antibacterial nanoparticles, removal of organic dye and so on have been reviewed. Finally, the advanced research questions of established techniques and relevant methodologies are identified constructively in order to achieve our specific goal.

Chapter 2 demonstrated the optical properties – SPR (Surface Plasmon Resonance), theoretical derivation of Mie extinction, scattering, absorption and field enhancement of single spherical plasmon as well as plasmon coupling effect using analytical and numerical methodologies. Single gold spherical nanoparticle has been used for the analytical model to classify the fundamental parameters of optical properties by deviating the diameter and refractive indices of their particles. Later, Finite Difference Time Domain numerical model for spherical silver nanoparticles is applied to identify their effective parameters such as absorption, scattering and distribution of charges of their electric field. The ultimate objective of this chapter is to address the optical properties of plasmonic nanoparticles in the treatment of wastewater for key detection and possible removal of Plasmon through simulation.

Chapter 3 explained the theoretical approach and necessary tools to characterize accurately the size, shape, crystal structure, element composition, and other physical properties of nanomaterial in wastewater management. This chapter has been divided into the following sections - XRD (X-ray diffraction), AAS (Atomic Absorption Spectrometry), Fluorescence Spectroscopy and Microscopy, FTIR (Fourier Transform Infrared) Spectroscopy), UV (Ultra Violet) Visible Spectroscopy, FESEM (Field Emission Scanning Electron Microscopy) and Zeta Potential covering the essential concept of some reliable methods to identify the unique properties of nanoparticle.

Chapter 4 covered the pH, FTIR, AAS, fluorescence spectroscopy of various water samples with graphs, parameters and images required for the experimental result analysis. We focused

on using these fundamental properties in the field of potential applications of plasmonic nanotechnology to contaminate our country's wastewater, Bangladesh. Multiple sources of water such as lake water, textile industry, pharmaceutical industry, and tap water have been taken to perform our research study. The purpose of this experimental result is to develop the convenient plasmonic property method for the treatment of wastewater.

Chapter 5 concluded the study of the thesis including a description of our significant achievements along with recommendations and potential drawbacks. Finally, to expand these novel concepts for the eradication of water resource scarcity in Bangladesh, the future opportunities has been presented with strong remarks.

Chapter 2

Theory and simulation of surface plasmon resonance and plasmon coupling

2.1 Introduction

In this chapter, the optical properties for plasmonics nanoparticles, particularly for single spherical gold (Au) and coupled silver (Ag) dimer have been outlined. Initially, Mie theory is applied effectively to observe the analytical model including scattering, absorption and extinction of single gold Nano spherical Plasmon since Mie scattering can only provide the spherical molecule theorem and fails to determine the theorem of other varieties shapes. However, the FDTD (Finite Difference Time Domain) numerical simulation approach has been shown to observe the coupling effect and field enhancement properties in order to clarify the key problem and address the coupling impact of two Nano plasmonic spherical silver particles.

Plasmonics nanoparticle has become rapid rising research field for the optical characteristics and fabrication of metal nanoparticles of different size, shape, structure, and tunable Plasmon resonances [50, 54, 62]. Plasmonic nanoparticles (PNPs)- along with gold (Au), silver(Ag), platinum(Pt) are exceedingly effective at optical properties such as extinction, absorption and scattering [50, 54].By changing the size, structure and nature, the optical response can be modified from the ultraviolet and through the visible to the electromagnetic range near-infrared locations [54].

The remaining portion of this chapter demonstrates Surface Plasmon Resonance, Localized Surface Plasmon resonance, Mie theory of optical characterization – extinction, scattering and absorption cross-sections, analytical study on the optical characteristics of single plasmonics Nano sphere – deviated by their refractive indices and particle's diameter, Finite Difference Time Domain simulation of plasmonic nanosphere dimer and their simulation results to investigate the coupling effect as well as field enhancement properties. These

theoretical optical characterizations of plasmonics nano particle adequately emphasize on the experimental part that has been discussed in chapter four and five.

2.2 Surface Plasmon Resonance (SPR)

2.2.1 Introduction to Surface Plasmon Resonance

Surface Plasmon Resonance (SPR) is considered as one of the tremendous optical property of plasmonic nanoparticle. Initially, the electromagnetic field may induce a resonance of free electrons over the molecule while the incident light wavelengths are much larger than metal nanoparticles (Figure-2.1), known as Surface Plasmon Resonance (SPR) [63, 64]

German Physicist, Gustav Mie first introduced Surface Plasmon Resonance in 1908 [64].For a spherical metal nanoparticle of much smaller size than the wavelength of light, the Plasmon oscillation interface is determined by the dipolar mode with α polarizability.

$$\alpha \text{ (polarizability)} = \frac{3\varepsilon_{oV(\varepsilon-\varepsilon_m)}}{\varepsilon+2\varepsilon_m} \qquad [2.1]$$

Where εo is the vacuum permittivity, ε_m is the dielectric constant of a medium and V is the particle volume. For Gold (Au) and Silver (Ag), strong SPR occur when electromagnetic frequency, ω is at visible frequencies where,

$$\varepsilon_r = -2\varepsilon_m \qquad [2.2]$$

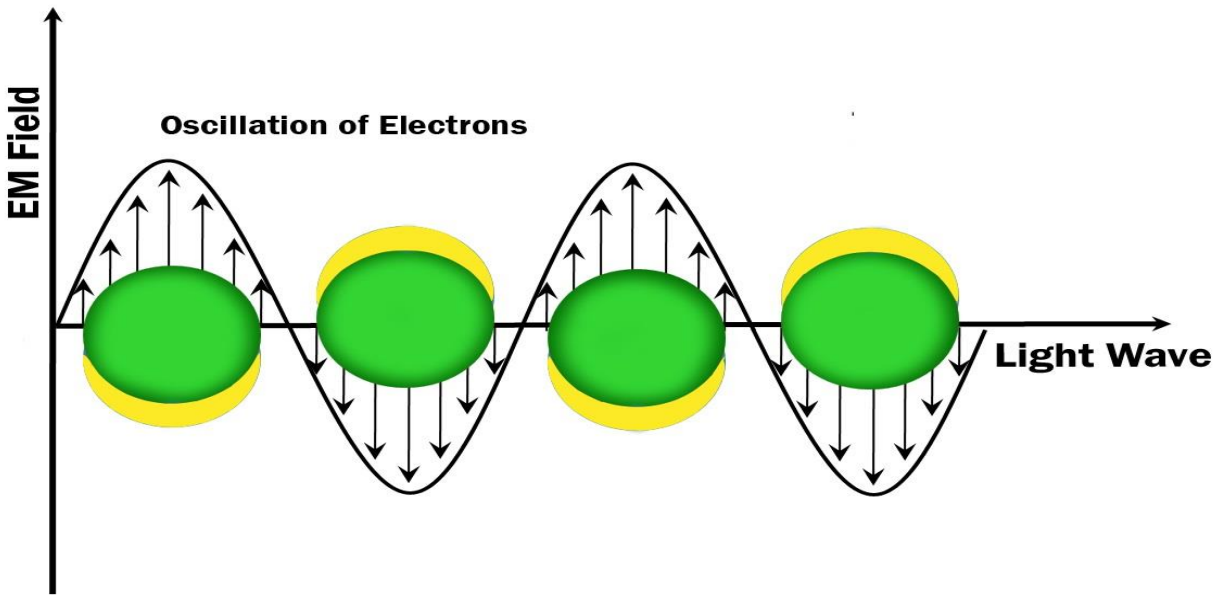

Figure-2.1: A schematic structure of electron oscillation of Nano sphere Plasmon and LSPR occurrence where Y-axis represents the Electro Magnetic (EM) field and X-axis represent the wave of visible light.

2.2.2 Localized Surface Plasmon Resonance (LSPR)

LSPR (Localized Surface Plasmon Resonance) charge density oscillation is basically observed by metallic plasmonics nanoparticle [63]. Localized surface plasmon are excited at an incident wavelength by an electric field which aggregates a strong scattering of light, emergence surface plasmon absorption bands and Electromagnetic (EM) field enhancement (Figure-2.1). By observing the wavelength of scattering and absorption, we can characterize the surface plasmon such as size distribution, shape and environment surrounded by them [63-65]. The upgrade properties of LSPR have been created strongly interest of this field which centered the exploitation of metallic framework as waveguides, as optical transmission, data capacity, and Nano photonic gadgets; as resonant light scatters (utilized within the diverse near-field filtering optical microscopies) and at long last as numerous sensors.

2.3 Theory of Extinction, Scattering and Absorption Cross section

Plasmonics nanoparticles have promptly become the subject of several studies for many years because of their optical, electrical and thermal properties [55, 65, 66]. Extinction, Absorption and Scattering cross sections obtain the most prominent optical properties of Plasmon At SPR, most photons are either absorbed or scattered at the metal or dielectric interface and consequently reflected light is significantly attenuated [66]. In plasmonics, the efficient level in which energy is absorbed from the incident plane wave is called the absorption cross section when SPR occurs [55, 67]. Again, scattering cross section occurs when the plasmonics radiation occurs due to SPR or LSPR [55, 67]. These, optical properties can be observed following Mie and Rayleigh theory [51].

2.3.1 Mie & Rayleigh theory

Rayleigh scattering and the Mie principle are the two main methods for measuring the absorp tion and scattering of nano particle cross sections [68]. Rayleigh scattering deals with the process where the light's wavelength is much greater than the particle size [69]. As the wavelength of the light produced by the light source goes from 200 nm to 1000 nm, and the

silver nanoparticles are being used are 25 nm in diameter, concern over the wavelength being one order of magnitude larger than the diameter ruled out use of Rayleigh scattering. Mie theory meanwhile is valid for all ratios of the nanoparticle diameter to the wavelength of the light [68, 69].

Mie theory or Mie scattering is an explanatory arrangement of Maxwell's equations for the scattering of electromagnetic radiation by particles of any measure (especially sphere) [51, 54, 56, 57]. Mie theory is commonly used in circular nanostructure electrical simulations; the properties of LSPR nanoparticles are modeled by generalized Mie theory. Mie scattering derives the scattering of an EM plane wave by a homogeneous spherical particle using Maxwell's equations [56, 57, 68].

2.3.2 Mathematical Calculation of Mie Theory

We consider the scattering of a polarized plane wave against a sphere with radius a (Figure-2.2).

As our main consideration of Mie theory is related to water application, an incoming plane wave with time dependence Magnetic field [H (x, y, z, t)] and Electric field [E (x, y, z, t)] hits the drop of water and creates the scattered radiation. Where,

μ – Relative permittivity of magnetic characteristics;

ε – Permittivity of electric characteristics;

The material properties $\mu 2$ and $\varepsilon 2$ inside a sphere of radius at the drop of water and the value $\mu 1$ and $\varepsilon 1$ outside the sphere in the air.

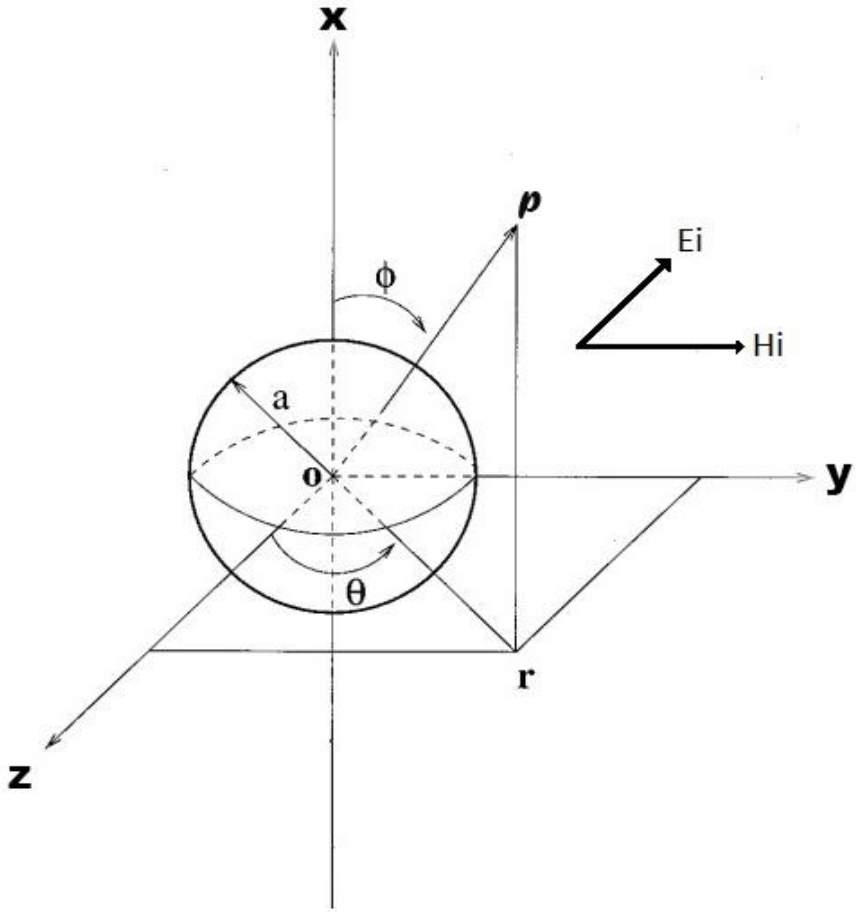

Figure- 2.2: A schematic diagram for the scattering of a polarized EM wave by a Gold Nano sphere of radius a. The positive X- axis represents the direction of propagation of incident wave and Y-axis represents the direction of EM field.

- Relation between dielectric constant and the refractive index

Mie scattering requires the refractive index and dielectric constant of the Nano sphere particle [54, 70]

A particle's index refraction (n) is known as the ratio of the speed (c) of light in the air or empty space to that particle's speed (c_m) of light.

$$n\ (refractive\ index) = \frac{c}{c_m} \quad [2.3]$$

Using Maxwell's equation, relative refractive index (n_r) in terms of the electric permittivity (ε) and magnetic permeability (μ) of the particle is

$$n_r = \left(\frac{\mu_{o\varepsilon_o}}{\mu_{o\varepsilon}}\right)^{-\frac{1}{2}} = \left(\frac{\varepsilon}{\varepsilon_o}\right)^{\frac{1}{2}} \quad [2.4]$$

Dielectric constant, $\varepsilon_m = \frac{\varepsilon}{\varepsilon o} = n^2$ [2.5]

However, this relation is considered for the real part of dielectric constant and refractive index.

Complex variable of refractive index, $m = n(1 - i\kappa)$ where nκ is the damping factor while κ is called the absorption index or the attenuation index [70-72].

The index of refraction is modified using Drude model by scattering surface of the electrons because for sphere nanoparticle main free path, $l_{eff} = 4/3R$ is much smaller than the large bulk material [66]. Drude model explains that complex dielectric function consists of bound electrons, $C_1 \; and \; C_2$ as well as the conduction electrons, $D_1 \; and \; D_2$[72], as in following equations :

$$\varepsilon_d(f) = \varepsilon_1 + j\varepsilon_2 = (C_1 + D_1) + j(C_2 + D_2) = 2n\kappa j + (n^2 - \kappa^2) \quad [2.6]$$

$$D_1 = 1 - \left(\frac{\omega_p^2}{\omega_r^2 + \omega_o^2}\right) \; and \; D_2 = \frac{\omega_p^2 \omega_o}{\omega_{r(\omega_r^2 + \omega_o^2)}} \quad [2.7]$$

Plasma frequency, $\omega_p = 4\pi N e^2 m *$.When the atoms have broken down into positive and negative charges then the state is called plasma which created plasma oscillation or frequency while m* is the effective mass of an electron and N is the density of electron. Moreover, ω_r is the frequency of collision, where $\omega_r = \frac{1}{t_s}$. ω_o is being modified to determine $\varepsilon_1 \; and \; \varepsilon_2$ in terms of the radius of Nano sphere, R and fermi velocity, v_{fermi}. $\omega_o(modified) = \omega_o + \frac{v_{fermi}}{R}$.

From equation 2.6 and 2.7, modified dielectric function using Drude model can be expressed as $\varepsilon_1 = 1 - \left(\frac{\omega_p^2}{\omega_r^2 + \kappa^2}\right) + \frac{\omega_p^2 \kappa}{\omega_{r(\omega_r^2 + \kappa^2)}}$ [2.8]

$$\varepsilon_d(f) = \varepsilon_1 + j\varepsilon_2 = 1 - \left(\frac{\omega_p^2}{\omega_r^2 + j\kappa}\right) + j\varepsilon_2 \quad [2.9]$$

- Bessel &Riccati functions

Cylindrical Riccati function (ψ_r) and spherical Bessel function (ξ_r) are defined as following expressions

$$\xi_{r(z)} = z\left[J_{r(z)} - jy_{r(z)}\right] \qquad [2.10]$$

$$\psi_{r(z)} = zJ_{r(z)} \qquad [2.11]$$

Where z is a size parameter and r is a number of order in summation index where r € N. Complex Bessel function of sphere has real part ($J_{r(z)}$) and imaginary part ($y_{r(z)}$).

$$J_{r(z)} = \sqrt{\frac{\pi}{2z}}J_r + \left(\frac{1}{2}\right)z \qquad [2.12]$$

$$y_{r(z)} = \sqrt{\frac{\pi}{2z}}y_r + \left(\frac{1}{2}\right)z \qquad [2.13]$$

From equation 2.12 and 2.13, evaluating ψ_r&$\xi_r$are **Riccati-Bessel functions**

$$\xi_{r(z)} = \text{Z}\left[\sqrt{\frac{\pi}{2z}}J_r + \left(\frac{1}{2}\right)z - \text{j}\sqrt{\frac{\pi}{2z}}y_r + \left(\frac{1}{2}\right)z\right] \qquad [2.14]$$

$$\psi_{r(z)} = z\sqrt{\frac{\pi}{2z}}J_r + \left(\frac{1}{2}\right)z \qquad [2.15]$$

The extinction cross section is a combination of the scattering cross section and the absorption cross section, according to Mie's theory [51, 54, 70]. For any required wavelength, these cross-sections can be measured.

$$Q(mie_{abs}) = Q(mie_{ext}) - Q(mie_{scat}); \qquad [2.16]$$

The Mie scattering cross sections is defined as

$$Q(mie_{scat}) = \left(\frac{2\pi}{k^2}\right)\sum_{r=1}^{\infty}(2r+1)(|a_r|^2 + |b_r|^2) \qquad [2.17]$$

Moreover, Mie extinction cross section is defined as

$$Q(mie_{ext}) = \left(\frac{2\pi}{k^2}\right)\sum_{r=1}^{\infty}(2r+1)Re(a_r + b_r) \qquad [2.18]$$

In these equations, a_r and b_r are extension coefficients of scattering. From equation, 2.14 and 2.15, extension coefficients of scattering are

$$a_r = \frac{m\psi r(mz)\psi r(z) - \psi r(mz)\psi`r(z)}{m\psi`_r(mz)\xi_r(z) - \psi_r\ (mz)\xi`_r(z)} \qquad [2.19]$$

$$b_r = \frac{\psi`r\ (mz)\psi r(z) - m\psi r(mz)\psi`r\ (z)}{\psi`n(mz)\xi r(z) - m\psi r(mz)\xi`r\ (z)} \qquad [2.20]$$

$z\ (size\ parameter) = kR$, R is the radius of Nano sphere particle. $m = \sqrt{\varepsilon}_m = n_r = \frac{n}{N}\psi r$ &$\xi_r$are **Riccati-Bessel functions**. K is the wavenumber and defined in terms of wavelength, λ. $Wave\ number, k = 2\pi N/\lambda$, where N can be defined as the refractive index of the particle.

To conclude, by evaluating the mathematical calculation of Mie theory the cross sections of extinction and scattering can be obtained of plasmonic nano sphere. In addition, Mie cross sections of absorption can be obtained by the difference of $Q(mie_{ext})\ and\ Q(mie_{scat})$. Finally, using the Maxwell's formulation, the analytic expressions for the single-scattering properties of the plasmonic Nano sphere particle has been derived, which include the scattering, absorption and extinction efficiencies.

2.4 Analytical study on the optical properties of single plasmonic nano sphere

Plasmon resonances at optical frequencies created strong scattering field of visible light range (420nm-750nm) with resonant peak wavelength which is highly sensitive to nanomaterial shape, size and local enhanced field [63, 67, 73]. With the help of Mie theory calculation, the spectral termination of Plasmon nanoparticle has been studied numerically by utilizing analytical code of scattering cross section while varying the complex dielectric function of Plasmon nanoparticle included an empirical parameter. Significantly, Mie scattering can accurately determine the dipole and higher resonant energies in terms of local field environment and size, shape [67, 73, 74]. However, Mie scattering cannot determine the resonant line widths of LSPR when the radius of particle is less than 20nm [67]. In this study, considering single Gold (Au) Nano sphere Plasmon to study the analytical method of the optical properties using Mie scattering calculation.

2.4.1 Optical properties of Single Nano Plasmon – Gold (AuNPs)

Gold nanoparticles, due to their stability and optical properties, are one of the most widely used nanoparticles. AuNPs have been one of the most commonly used nanoparticles because of their optical properties and solidity [64, 67, 75]. Numerical study is based on Single AuNPs because of several advantages. Firstly, suppression of inhomogeneity occurs which

provides significant surface defects, chemical composition as well as some size, shape parameters [66, 73]. Secondly, Single AuNPs tests neighborhood properties and chemical situations without considering the over diffuses and inter-particle intuitive. The LSPR spectrum can be directly compare with the calculated Mie scattering, which addresses the effective results of aggregation on the optical properties. Moreover, spherical AuNPs absorbing light is starting from around 520nm to longer wavelength as the radius of nanomaterial increases while bigger AuNPs owing larger cross sections which can be an excellent property of strong electronic contrast [67, 76, 77].

To observe the single Plasmon properties of AuNPs, Numerical simulation has been experimented using Wolfram Mathematica 12.0.0. The linear relative dielectric function of Au is expressed from Johnson and Christy (optical constant n and k) [53]. We investigated single particle properties by varying their dielectric constant, $\varepsilon_m = n^2$and our main concern is to determine the plasmonics in water, we characterized the effect of scattering cross sections by differentiating the diameter of when dielectric medium is 1.33 (water) of 40nm AuNPs.

2.4.2 Analytical simulation of AuNPs, as a function of refractive indices, n

In this section, the numerical analytical result has been presented to observe how an absorbing medium can affect the scattering while considering eight different sets of indexes of refraction for a single spherical AuNPs. Figure-2.4.2 represents the 40nm Au nanoparticle scattering properties for the refractive index of eight sets of absorbing medium where considering the real part of refractive indices (n = 1.00, 1.33, 1.50, 1.90, 2.00, 2.20, 2.50) and size parameter, z respectively.

Moreover, Figure-2.3 shows the effective variations of Mie scattering peak position. This inspection shows clearly when the refractive indices increases, the peak position of wavelength is red shifted (longer wavelength) of the Surface Plasmon resonance from around 530 nm to 820 nm. However, Cross-sectional scattering is directly proportionate to the refractive index, which means there is an improvement in scattering cross sectional area from (Table-1) $2.90657\ X10^{-15}m^2$ to $2.47029\ X\ 10^{-13}m^2$. The scattering efficiency approaches for 40 nm radius of gold nanoparticle when absorbing medium is water (n = 1.33), visible light range wavelength has been observed (570 nm) and color of reflection is indigo.

Noticeably, there are two peaks (690 nm and 820 nm) when refractive index is 2.50 (Silicon) which can be the characterization of spherical the Gold nanoparticle. The comparative study of Numerical simulation using single Gold Nano spheres (AuNPs) when varying the refractive indices, and has been referred in table-2.1.

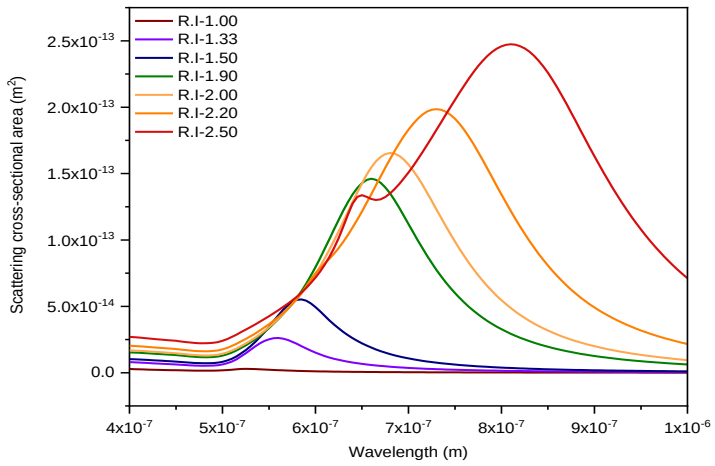

(i)

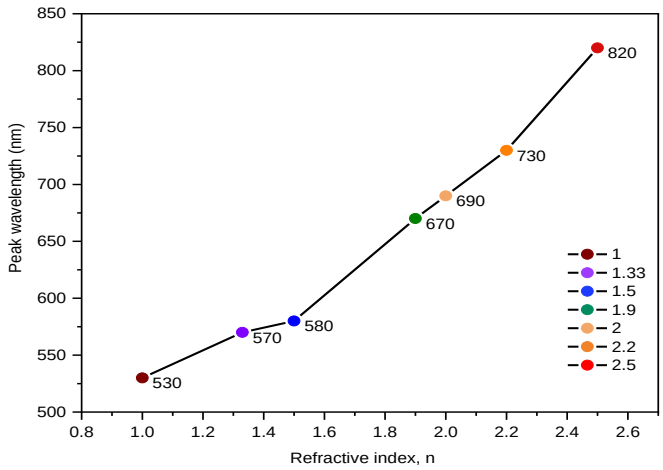

(ii)

Figure- 2.3(i) Mie scattering (Analytical) cross section spectrum of 40nm AuNS when varying refractive indices [Scattering cross-sectional area (m^2) vs Wavelength (m)]. Here, n = 1.00 - brown series, n = 1.33 – violet, n = 1.50 – blue series, n = 1.90 – green series, n = 2.00 – yellow series, n = 2.20 – orange series and n = 2.50 red series.(ii) Comparison of scattering effect – when varying single Au Nano sphere's radius (Peak wavelength vs Radius, R)

Refractive index, n	Scattering Cross-sectional area (m^2)	Peak of Wavelength(m)
1.00 (Air)	$2.90657\ X10^{-15}$	$5.3\ X10^{-7}$
1.33 (Water)	$2.60325\ X10^{-14}$	$5.7\ X10^{-7}$
1.50 (Glass)	$5.72723\ X\ 10^{-14}$	$5.8\ X\ 10^{-7}$
1.90 (Zircon)	$1.47713\ X\ 10^{-13}$	$6.7\ X\ 10^{-7}$
2.00 (Si_3N_4)	$1.66847\ X\ 10^{-13}$	$6.9\ X\ 10^{-7}$
2.20 (Diamond)	$1.98085\ X\ 10^{-13}$	$7.3\ X\ 10^{-7}$
2.50 (Silicon)	$2.47029\ X\ 10^{-13}$	$8.2\ X\ 10^{-7}$

Table-2.1: Comparative study of Gold nanosphere (AuNPs) when varying the refractive indices, n where column-1 represents refractive index, column-2 Scattering cross-sectional area and column-3 peak of wavelength

2.4.3 Analytical simulation of AuNPs, as a function of particle's diameter

A numerical analysis based on varying the AuNPs radius (R) when refractive index is 1.33-water as our experimental part is related to water. Figure-2.4.3 shows the single Au nanoparticle scattering properties by varying their radius (R =10nm, 40nm, 60nm, 80nm, 100nm) respectively. To perceive the observation, the same Mie scattering code has been used while refractive index is fixed which is 1.33 and varying the radius of gold nanoparticle. From the figure - 2.4, peak position of 10 nm Au is close to zero while scattering cross sectional area is $4.18448\ X\ 10^{-18}m^2$ and wavelength is 550 nm. However, for 100nm AuNPS multiple peak has been observed when wavelength is 565 nm and 770 nm. Additionally, the peak position of wavelength is red shifted from 550 nm to 770 nm when radius is 10 nm to 100 nm and the peak position of cross sectional area is increasing from $4.18448\ X\ 10^{-18}m^2$ to $2.20287\ X10^{-13}m^2$ (Table-1). The result indicates that, by increasing the radius of gold nanoparticle, we will get longer

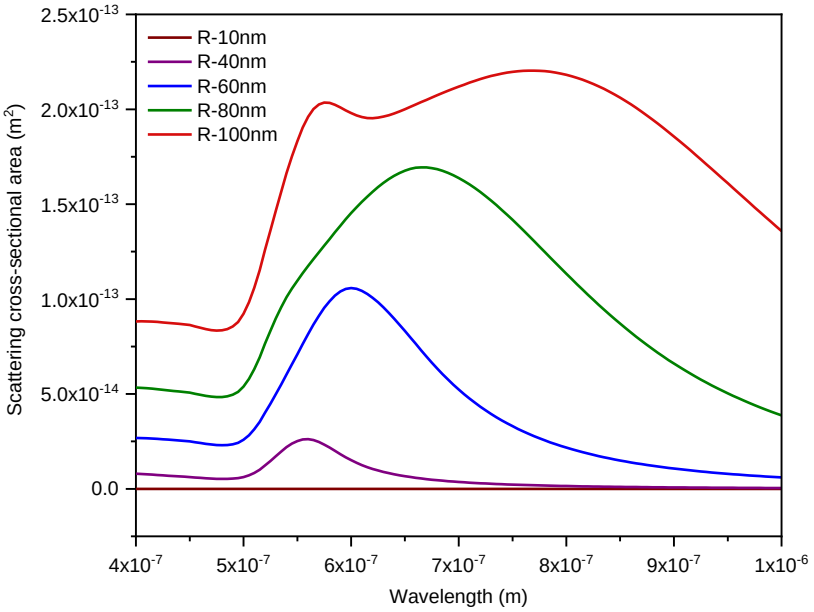

(i)

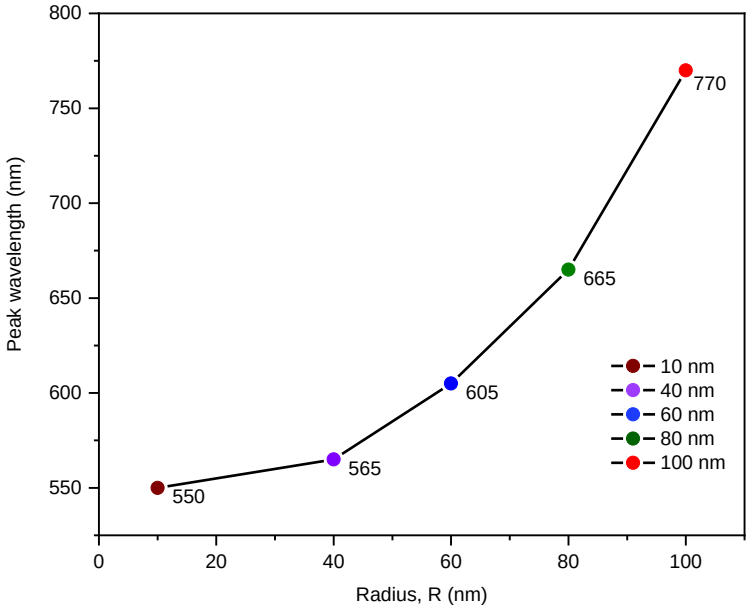

(ii)

Figure: 2.4 (i) Mie scattering (Analytical) cross section spectrum of AuNS as a function of particle's diameter when n – 1.33. [Scattering cross-sectional area (m^2) vs Wavelength (m)]. Here, R = 10nm – brown series, R = 40nm – violet series, R = 60 nm – blue series, R = 80 nm – green series, R =100nm – red series . (ii) Comparison of scattering effect – when varying single Au Nano sphere's radius (Peak wavelength vs Radius, R)

In conclusion, the calculated scattering spectrum distinctly represents the interrelation of plasmonics (Au) nanoparticle optical properties including scattering cross-section, surface Plasmon resonance (SPR) wavelength, extinction cross-section, and absorption scattering changes on refractive indices and sizes of nanoparticles where the measurement findings are consistent with previous observations [10-12, 20]. By increasing the size (radius) as of AuNPs from 10 to 100 nm and refractive indices from 1.00 to 2.50, the scattering cross section is rapidly increasing. The variation in wavelength maximum of Nano spheres, from 530 to 820 nm and the variation of scattering area, from $4.18448\,X\,10^{-18}m^2$ to $2.20287\,X10^{-13}m^2$ (Table-1). The comparative study of analytical simulation using single Gold nanosphere (AuNPs), when varying the radius of AuNS has been referred in table-2.

Radius, R (nm)	Scattering Cross-sectional area (m^2)	Peak of Wavelength(m)
10 nm	$4.18448\,X\,10^{-18}$	$5.5\,X\,10^{-7}$
40 nm	$2.57188\,X\,10^{-14}$	$5.65\,X\,10^{-7}$
60 nm	$1.05437\,X\,10^{-13}$	$6.05\,X\,10^{-7}$
80 nm	$1.69413\,X\,10^{-13}$	$6.65\,X\,10^{-7}$
100 nm	$2.20287\,X10^{-13}$	$7.7\,X\,10^{-7}$

Table-2.2: Comparative study of Gold nanosphere (AuNPs) when varying the radius, R where column-1 represents radius, column-2 Scattering cross-sectional area and column-3 peak of wavelength

2.5 Finite Difference Time Domain simulation of Silver nanosphere dimer (AgNS)

In this section, the comparative study of Scattering and absorption cross section spectrum of two plasmonics metal- silver Nano spherical dimer (AgNPs) using FDTD simulation has been evaluated. Cross-section extinction is the summation of the absorption and dispersion cross-section that can be discussed by FDTD numerical process [51, 54, 78, 79]. In these assessments, the width between two Nano spheres forming the dimer was varied to obtain the effect of nanoparticles spacing between the nanostructures on the electromagnetic fields in the regions [80]. In this observation, the coupling separation between two Nano spherical silver forming dimer is varied to evaluate the effect of cross-sectional area when absorbing medium is water (refractive index-1.33). In this simulation, we find an effective coupling

effect comparison when adjusting the separation distance between Silver nanoparticle's two 40 nm radiuses.

2.5.1 Specification of FDTD simulation setup

The layout editor demonstrates object simulation, total field, scattered field and polarization direction (Figure-2.5, 2.6). The two Ag Nano spheres are simulated in the middle and they are easily moveable with a mouse. These two Nano spheres are covered a yellow rectangular box with a total field (TF) surrounded by a white rectangular box with a total field scattered field origin (TFSF) and eventually a scattered field (SF) with an outer yellow rectangular box. (Figure-2.5).

A total scattered field source (TFSF) was used to simulate the Ag Nano spheres, which includ es Ag Nano spheres. Two research groups were used, first in the total field area and second in the scattered field area (Figure-2.5, 2.6). These analytical groups provide transversal absorption and scattering and angular distribution of scattered radiation. An improved frequency profile monitor for calculating the electrical field is included (Figure-2.5).

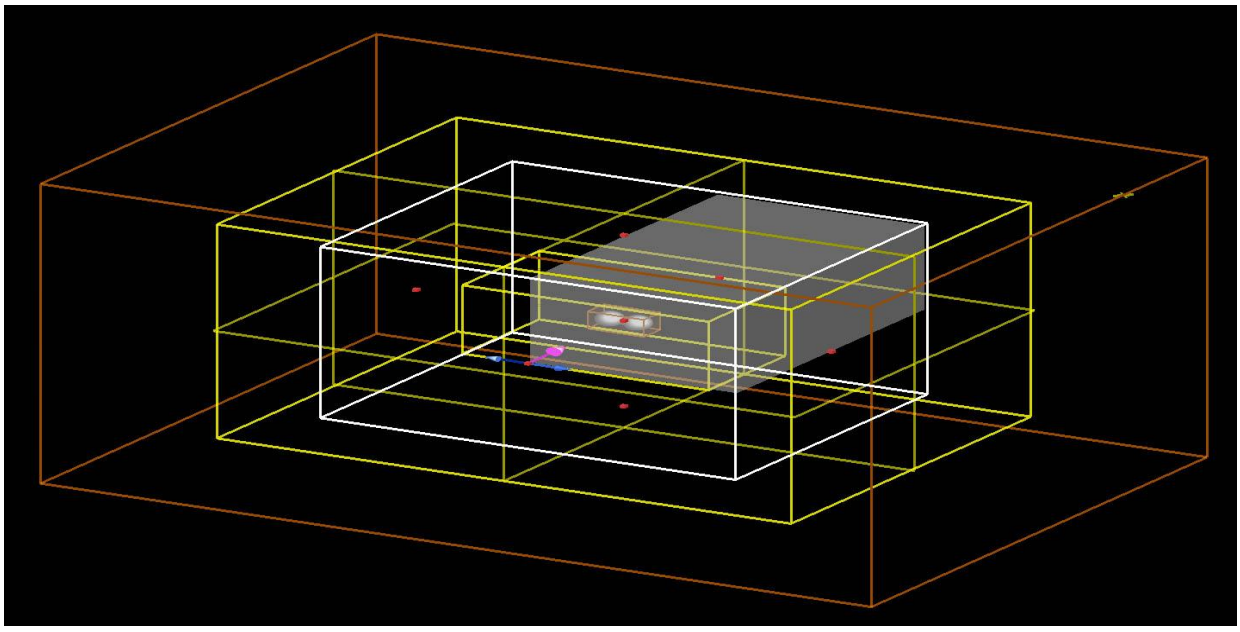

Figure 2.5 Layout editor of FDTD (finite difference time domain) simulation layout for Plasmonic two Nano spherical silver (Ag-palik) dimer (in the middle) – perspective view. The yellow rectangular box represents the TF (total field), the white rectangular box represents the TFSF (total - field scattered field) and finally, the outer yellow rectangular box represents the SF (scattered field). The pink bolt appears the propagation direction, k vector. The blue arrow represents the electric field direction.

To analyze the size effect, the linear effective dielectric function of Ag Nano spheres is expressed from Johnson and Christy's dielectric function [53]. The accuracy of location can be done by enlarging the mesh override region. Uniform mesh region is the best for curved surface and TFSF sources. Moreover, without giving space (~2 mesh cells) in sources, the field cannot be meaningful [81].

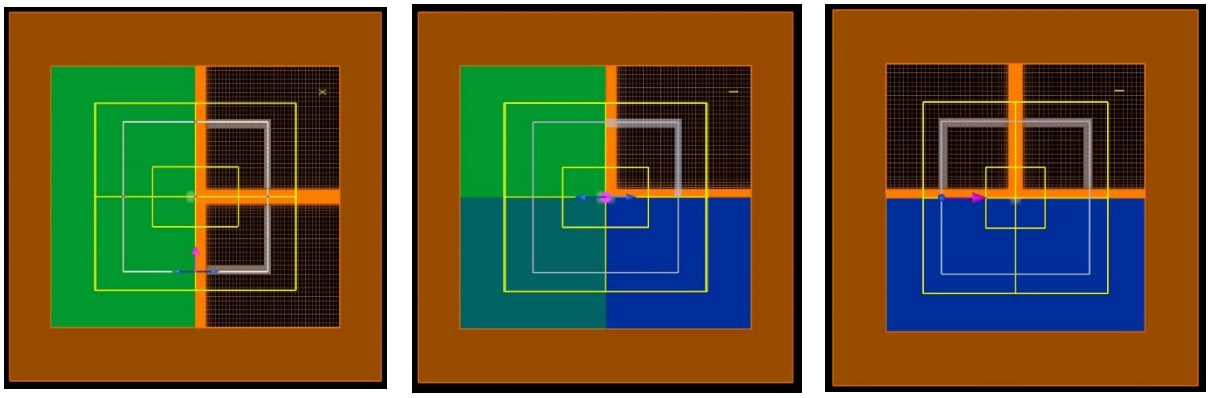

Figure 2.6 Layout editor of FDTD (finite difference time domain) simulation layout for Plasmonic two Nano spherical silver (Ag-palik) dimer– X-Z (Figure 2.6.1), X-Y (Figure 2.6.2), Y-Z (Figure 2.6.3) view. The yellow box represents the TF, the white box represents the TFSF and finally, the outer yellow box represents the SF.The pink and blue arrows represent the propagation direction and electric field.

However, another analysis group located outside the TFSF source observes the total scattering of power from the particle hence, the scattering cross section (Figure: 2.5, Figure: 2.6). Moreover, by considering the value of geometrical area $\pi \times r^2$ and the size parameter $2 \times \pi \times r^2$, scattering cross-section or absorption has been calculated.

To evaluate the coupling effect, Nano photonic FDTD simulation software- Lumerical FDTD solution.Inc has been used [82]. Absorption cross section is determined within the origin of Total field scatter field (TFSF) source. Likewise, the scattering cross section is determined located outside the TFSF origin and eventually extinguished by the summing up of the absorption and the scattering cross section determines the extinction cross section [75, 79].

The silver content is a version of the refractive index 1.33 (Water) and the "Ag Silver -Palik." The maximum scattered field source spans from a wavelength of 400 to 1000 nm. The default settings for system is adjusted in such a way that a reasonable accurate result is obtained with at a minimized simulation time. For obtaining results with higher accuracy, the grid resolution of mesh size is 0.5nm. Mesh size defines the smoothness of spectrum (Figure 2.7, 2.8), the less the mess size, the more accuracy of result [54, 79].The mesh refinement to

'conformal variant 1' to achieve sub-cell resolution for the silver particle boundary [79]. Symmetrical simulation has been used. The advantage of symmetry of the simulation is to decrease the simulation time and memory by a factor of four.

$$fpoint = length\frac{lambda}{1.47} \qquad [2.21]$$

2.5.2 Scattering cross section of 40nm AgNS dimer

Scattering cross section is a rate at which a particular plasmonics radiation occurs which is proportional to the target quantity[56, 79]. To investigate the scattering cross sectional coupling effect when separation distance is from 1nm-320nm, FDTD simulation method has been used.

Figure- 2.7.1 and Figure-2.8.1 show the scattering coupling effect when varying their coupling separation. This inspection shows clearly when the separation decreases, there has been a red shift (longer wavelength) of the Surface Plasmon resonance from around 452 nm to 771 nm. On the other side, there is an improvement in scattering cross sectional area from $6.90\,X\,10^{-14}m^2$ to $8.2\,X\,10^{-14}m^2$ when the separation decreases from 320nm to 1nm, which can be the observation of strong coupling and weak coupling. Additionally, two peaks of wavelength, one is very small and another is longer and red shifted, have been observed when coupled silver (Ag) Nano spherical plasmonics dimer is having strong coupling effect from 1nm – 8nm (Figure 2.7, Figure-2.8). However, the higher peak value is considering for comparative study of scattering and absorption cross section that is referred in Table-2.3.

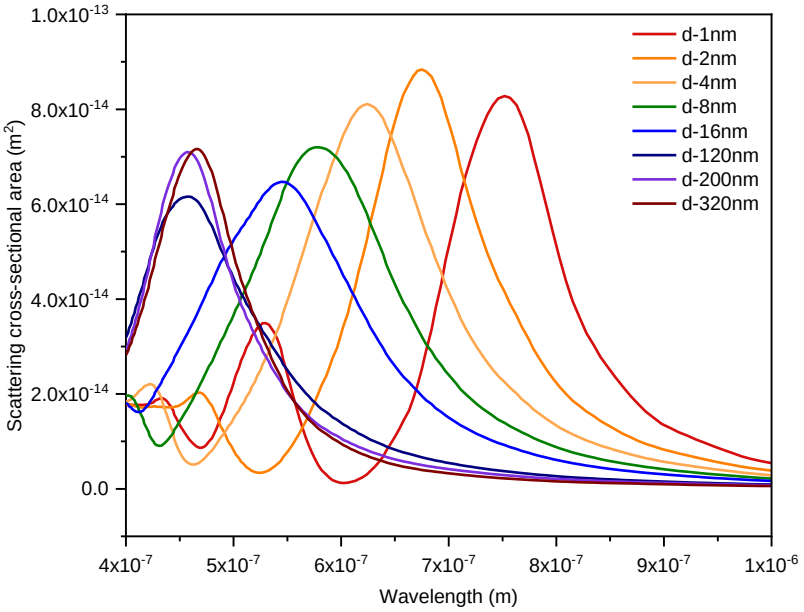

(i)

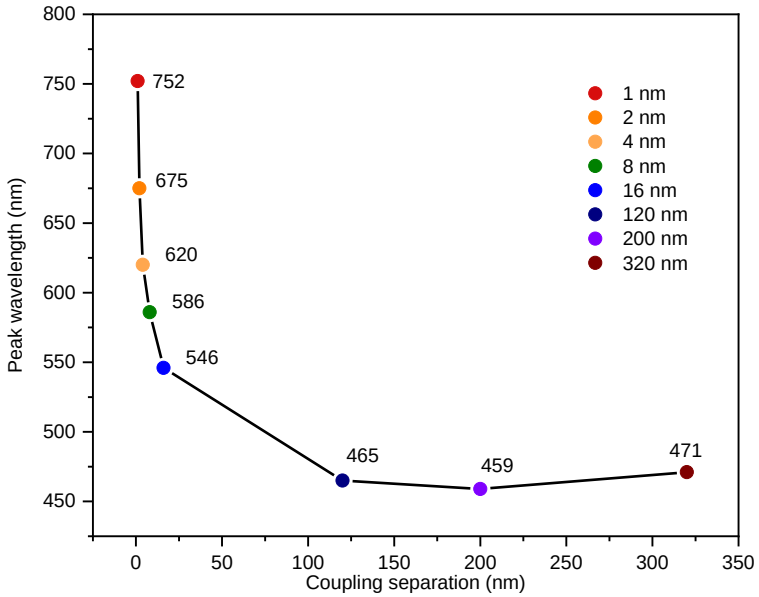

(ii)

Figure-2.7: (i) FDTD simulation results of 40 nm radius AgNS dimer Plasmon coupling scattering spectrum when separation distance, d = 1nm, 2nm, 4nm, 8nm, 16nm, 120nm, 200nm and 320nm .(ii)Plasmon scattering coupling effect – strong coupling to weak coupling of 40 nm radius AgNS dimer (Peak wavelength vs coupling separation, d)

2.5.3 Absorption cross section of 40nm AgNS dimer

The absorption cross section is the speed at which energy is absorbed from the incident plane wave [51]. To observe the absorption cross sectional coupling effect when separation distance is from 1nm-320nm, FDTD simulation method has been used. Figure- 2.7(i) shows the absorption coupling effect when varying their coupling distance. This inspection shows clearly when the separation decreases the red shift (longer wavelength) of the Surface Plasmon resonance from around 467 nm to 752 nm. On the other side, there is an improvement in absorption cross sectional area from $0.90\,X\,10^{-14}m^2$ to $2.8\,X\,10^{-14}m^2$ when the separation decreases from 320nm to 1nm, which can be the observation of strong coupling and weak coupling. However, scattering absorption cross section is much smoother compare to absorption scattering cross-section (Figure 2.7(i), Figure 2.8(i)).

2.5.4 Observation of AgNs dimer – strong to weak coupling

From this observation, a constructive coupling effect comparison occurred when adjusting the separation distance between two-40nm radius AgNPs between both two-40nm radius AgNPs between two-40nm radius AgNPs both for absorption and scattering cross sections. Figure-2.7(ii) and Figure 2.8(ii) clearly speaks that strong coupling occurs when separation distance is from 1nm to 8nm and for strong coupling, wavelength is red shifted. For scattering and absorption, the highest strong coupling is shown when peak value of wavelength is around (771nm -752nm). Moreover, when separation distance is 2nm, peak value of wavelength is 675nm (Figure.2.7 (ii)), 667nm (Figure. 2.7(ii)) which indicates that a simple variation of separation distance can effect in a great extent of coupling effect. On the other hand, weak coupling occurs from separation distance, d = 16nm, 120nm, 200nm (very weak). Ironically, at 320nm Ag Nano Plasmon acts like single particle. When separation distance is 320nm, peak wavelength is around 467nm (absorption) and 471nm (scattering) whereas for 40nm radius of silver nanoparticle peak absorption wavelength is around 465nm [81] which indicates that no coupling occurs for separation distance 320nm.

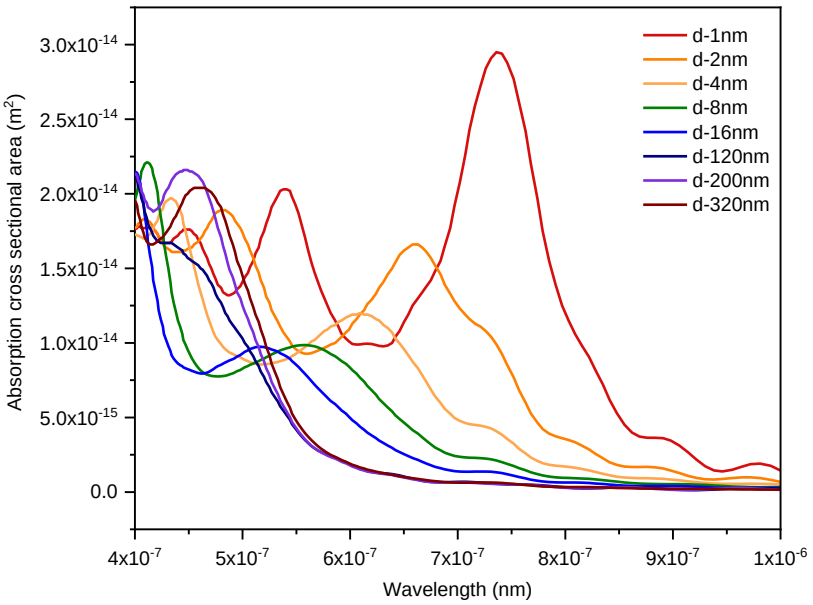

(i)

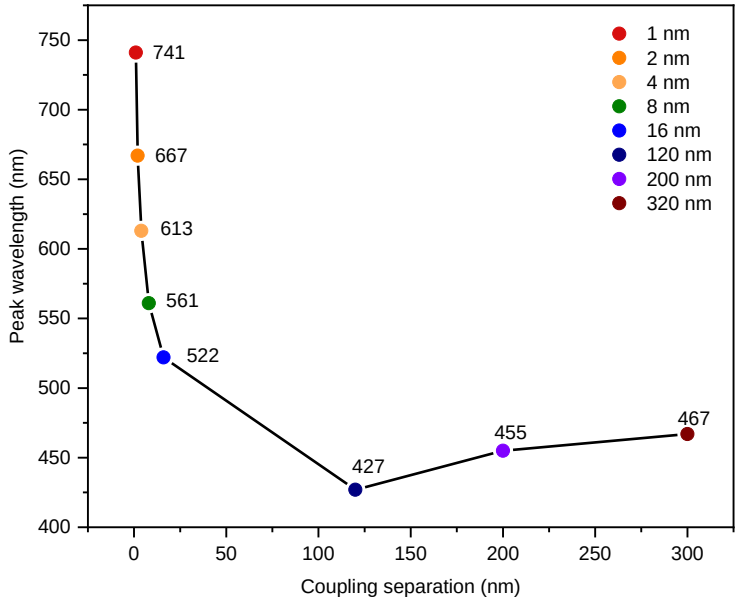

(ii)

Figure-2.8 (i) FDTD simulation results of 40 nm radius AgNS dimer Plasmon coupling absorption spectrum when separation distance, d = 1nm, 2nm, 4nm, 8nm, 16nm, 120nm, 200nm and 320nm.(ii) Plasmon scattering coupling effect – strong coupling to weak coupling of 40 nm radius AgNS dimer (Peak wavelength vs coupling separation, d)

To conclude, the scattering and absorption coupling effect of silver nano spherical plasmon can be efficient enough to determine the strong and weak coupling properties and from peak wavelength, we can compare the values with another single Nano Plasmon. The distance between two silver Nano spheres plays a vital role in peak and strength of scattering and absorption. As per table 2.3, it has been seen that as we are decreasing the separation distance between two silver Nano spheres the scattering peak wavelength is also being changed and it shows red shift in SPR peak. When the separation distance is maximum at 320 nm the scattering peak is at 464 nm, which is close to blue color (visible light spectrum) however, when the separation distance is 1 nm the scattering peak is at 752nm which is wavelength of red color. Therefore, a red shift in SPR peak will be observed for two silver nano spheres reducing the separation distance and so as if we increase the separation distance a blue shift in SPR peak will be observed. We have discovered the same behavior from the graph of absorption and extinction.

2.6 Theory of Plasmon's Field Enhancement

Electric field enhancement is considering one of the strong optical properties of Surface Plasmon Resonance for a metallic dielectric interface plasmonic nano materials are excited for photons [58]. Field enhancement is the ratio of the incident electrical field and local electrical field and plasmon has an optimum localization and electromagnetic field [59]. plasmonic NPs are smaller in dimension compared to the wavelength of the light, since this small dimension causes polarization with an induced charge distribution appearing from the plasmon surface causes a distribution of localized electrical field [58, 83, 84]. Again, the charge density and size and shape of the particle is much smaller than the wavelength, the local field distribution will enhance more that is bound to the surface plasmon resonance (SPR) [59, 61, 85].

Effective maximum field enhancement of a spherical particle can be found by following approximation,

$$\frac{E_s}{E_o} = 1 + \frac{|\varepsilon_{medium} - \varepsilon_o|}{|\varepsilon_{medium} + 2\varepsilon_o|} \qquad [2.22]$$

The charge distribution and field enhancement can calculate by utilizing Mie scattering or numerical direct simulations. In this section, FDTD (Finite Difference Time Domain) method

has been used to over view the strong coupling field enhancement of 40nm AgNS dimer. Additionally, how coupling effect can increase the charge distribution and local field enhancement is also discussed.

2.6.1 Field Enhancement of 40nm AgNS dimer – FDTD simulation specification

In our simulation, we used FDTD software (Lumerical solutions, Inc 8.15.736, Canada). We ran the simulation with a total-field scattered field source (TFSF) ; its wavelength varying from 400 nm to 1000 nm and grid resolution of 0.5nm for getting a clear electric field distribution. In our FDTD simulation analysis, we used two silver – Palik (0-2µm) Nano spheres each of them having 40 nm radius with refractive index of 1.33 (refractive index of water). Figure.2.8 shows the spatial distribution of Electric field as a function of incident light, when the incident E-field is polarized along the axis of two 40 nm radius silver spheres.

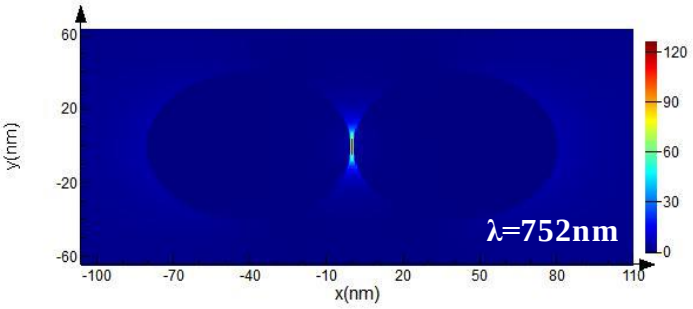

(i)

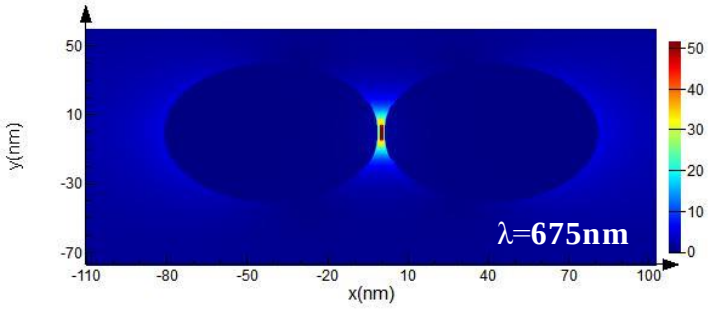

(ii)

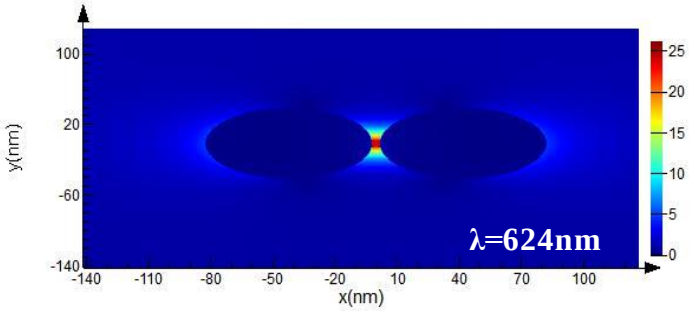

(iii)

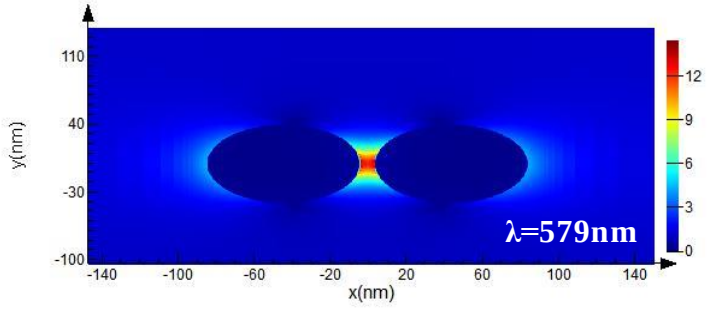

(iv)

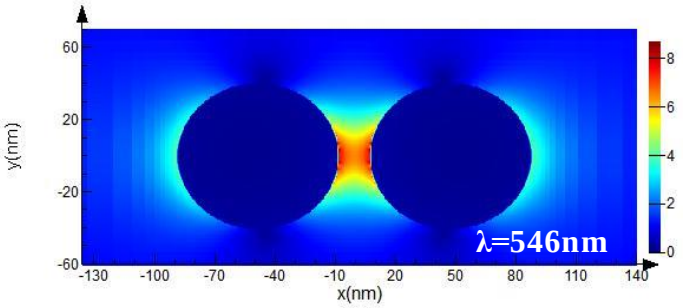

(v)

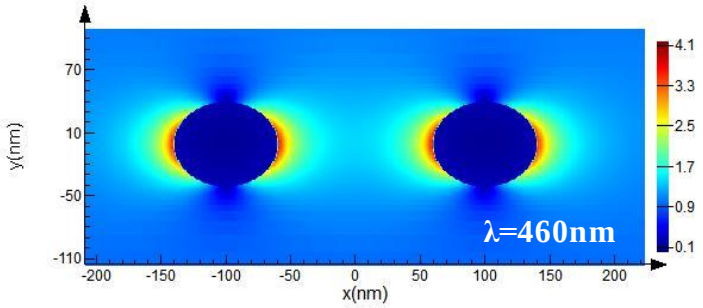

(vi)

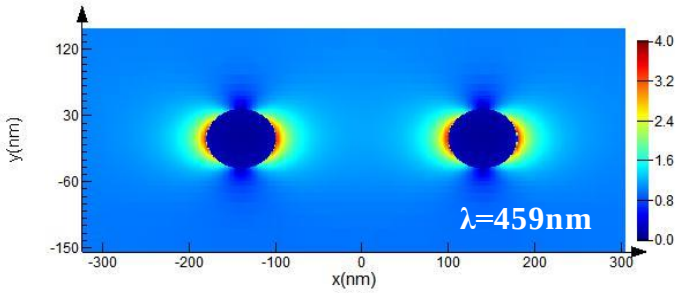

(vii)

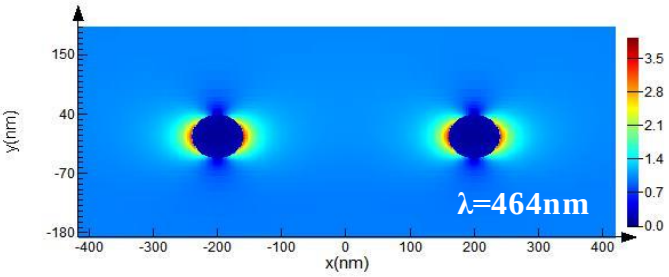

(viii)

Figure-2.9: Field Enhancement of 40nm Ag Nano sphere when separation distance is varying. (i) for 1 nm, (ii) for 2 nm ,(iii) for 4 nm, (iv) for 8 nm(v) for 16 nm, (vi) for 120 nm, (vii) for 200 nm and (viii) for 320 nm of X-Y plane respectively with the scattering peak value

Here, we can observe that the electric field enhancement is varying from 120 au to 3.5 au gradually when spacing between the silver Nano spheres are increasing from 1 nm to 320 nm. Figure-2.9(i) shows electric field enhancement intensity of 120 au when separation distance is 1 nm among the two Nano spheres at resonance peak 752 nm. Figure- 2.9(ii) shows an electric field enhancement intensity of 50 au when the separation distance is 2 nm at resonance peak 675 nm. Furthermore, Figure-2.9(iii) shows an electric field enhancement intensity of 25 au when the separation distance is 4 nm at resonance peak 624 nm. Figure-2.9(iv) shows an electric field enhancement intensity of 12 au when the separation distance is 8 nm at resonance peak 579 nm. Figure-2.9(v) shows an electric field enhancement intensity of 8 au when the separation distance is 16 nm at resonance peak 546 nm. Figure-2.9(vi) shows an electric field enhancement intensity of 4.1 au when the separation distance is 120

nm at resonance peak 460 nm. After then, Figure-2.9 (vii) shows electric field enhancement intensity of 4 au when the separation distance is 200 nm at resonance peak 459 nm and finally Figure-2.9(viii) shows electric field enhancement intensity of 3.5 au when the separation distance is 320 nm at resonance peak 464 nm. Here, we can clearly observe that when the separation distance is smaller the electric field enhancement is greater which is due to near field. However, when the distance is larger than around 2.5 times than the radius of Nano spheres, it shows far field characteristics as a result the electric field is too weak compare to near field intensity.

2.6.2 Electric Field Intensity of 40 nm AgNS dimer

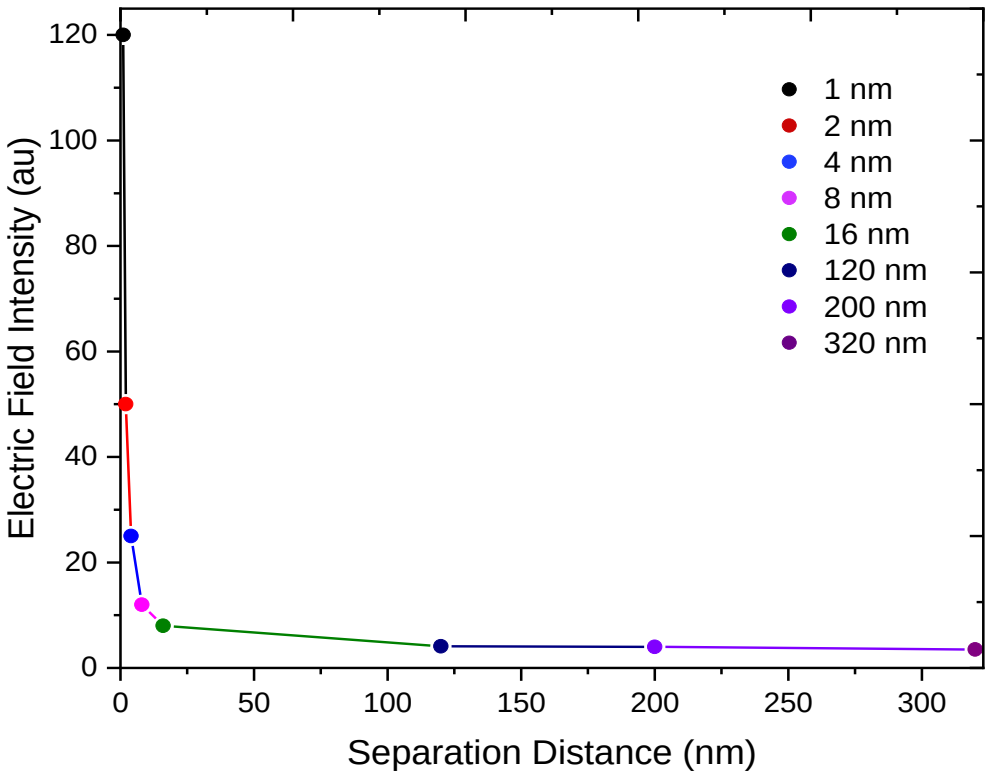

Figure-2.10: Separation distance between two AgNS dimer vs Electric Field intensity using FDTD simulation

It has been seen that by varying the separation distance in x-axis, we get a clear change in electric field intensity. While we are changing the separation, distance from 1 nm to 4 nm the change in y-axis is almost vertical which is due to near field effect. As we know that strength

decrease around inverse-distance squared with increasing distance for near field electric field strength. However, after separation distance of 100 nm there is very little change in electric field intensity and the electric field is too weak compare to near field as far-field strength decreases inversely with the distance from the source.

Separation Distance (nm)	Scattering		Absorption		Extinction		Field Enhancement		
	cross-sectional area(m^2)	Peak of wavelength (m)	cross-sectional area(m^2)	Peak of wavelength (m)	cross-sectional area(m^2)	Peak of wavelength (m)	X	Y	Z
1	$8.28 X10^{-14}$	$7.52 X10^{-7}$	$2.95 X10^{-14}$	$7.36 X10^{-7}$	$1.11 X10^{-13}$	$7.46 X10^{-7}$	120	120	120
2	$8.84 X10^{-14}$	$6.75 X10^{-7}$	$1.89 X10^{-14}$	$6.81 X10^{-7}$	$1.04 X10^{-13}$	$6.70 X10^{-7}$	50	50	50
4	$8.11 X10^{-14}$	$6.24 X10^{-7}$	$1.20 X10^{-14}$	$6.09 X10^{-7}$	$9.27 X10^{-14}$	$6.24 X10^{-7}$	21	25	25
8	$7.20 X10^{-14}$	$5.79 X10^{-7}$	$9.86X10^{-15}$	$5.58 X10^{-7}$	$8.15X10^{-14}$	$5.76X10^{-7}$	10	12	12
16	$6.47 X10^{-14}$	$5.46 X10^{-7}$	$9.71X10^{-15}$	$5.2 X10^{-7}$	$7.37 X10^{-14}$	$5.43 X10^{-7}$	5	8	8
120	$6.16 X10^{-14}$	$4.60X10^{-7}$	$1.53X10^{-14}$	$4.57X10^{-7}$	$7.69 X10^{-14}$	$4.55 X10^{-7}$	50	50	50
200	$7.1 X10^{-14}$	$4.59 X10^{-7}$	$2.16 X10^{-14}$	$4.47 X10^{=7}$	$9.23 X10^{-14}$	$4.57 X10^{-7}$	1	4	4
320	$7.16X10^{-14}$	$4.64 X10^{-7}$	$2.04 X10^{-14}$	$4.6 X10^{-7}$	$9.19 X10^{-14}$	$4.65 X10^{-7}$	0.9	3.5	3.5

Table-2.3: FDTD simulation of Silver nanosphere dimer (AgNPs) including scattering, absorption, extinction and field enhancement.

Lastly, the comparative study of scattering, absorption, extinction and field enhancement for two 40 nm AgNS dimer coupling separation distance using numerical FDTD simulation has been illustrated in Table-2.3. Table-2.3 overviewed the whole summary of result found in FDTD simulation.

2.7 Conclusion

In this chapter, we evaluate the optical characteristics such as SPR (Surface Plasmon Resonance), Mie scattering, extinction and absorption properties using single AuNS analytical method as well as numerical Finite Difference Time Domain (FDTD) simulation of two-coupled AgNS dimer. We also identify the charge distribution and field enhancement which differs their coupling separation distance from two coupling AgNS dimer. In conclusion, using analytical method and numerical method, a noteworthy relationship has been observed between the shape, size and optical characteristics of plasmonic nano particle. Increasing size induces red shift of absorption, scattering and extinction and decreasing coupling separation distance maximizing the intensity of the electromagnetic field of coupled two silver nano spherical dimer. In order to implement plasmonic molecules in wastewater treatment, the following experimental chapters have been using these optical properties to characterize the plasmonic nanoparticle.

Chapter 3

Theory and technique for characterization of nanomaterials

3.1. Introduction

Several techniques have been utilized to characterize the size, shape, crystal structure, elemental composition and an assortment of other physical properties of nanoparticles. In this section, we will discuss briefly some techniques to characterize the nanoparticles. The techniques that are used to the characterization of nanomaterial generate images that indicate different material's characters. Mainly the picture types are two sorts, like microscopy and spectroscopy. The generation of an image of the nanoparticle by these techniques varies. Microscopy strategies create pictures of individual nanoparticles to represent their shape, size, and area. Spectroscopy, which estimates the particles' cooperation with electromagnetic radiation as a component of wavelength, is helpful for certain classes of nanoparticles to indicate concentration, size, and shape. X-ray diffraction (XRD), Field emission scanning electron microscopy (FESEM), Transmission electron microscopy (TEM), Surface area analysis, Fourier transform infrared spectroscopy (FTIR), UV visible, Zeta potential, Atomic absorption, etc. are the popular techniques for the characterization of nanoparticles.

3.2 X-ray diffraction (XRD)

The structural features of any nanoparticle are essential for identification. X-ray diffraction technique is widely used to do the task. XRD determines at least one-dimensional structure range from 1-100nm. By XRD test particle can be identified by its atomic arrangements at interfaces. Powder or single crystal can experiment by XRD. X-rays scattering and Bragg diffraction can access the morphological and structural information of the investigated nanomaterials. Among the others we quote[86]:

- Crystal atomic structure: positions/symmetry of the atoms in the unit cell, unit cell size, size/shape of the monocrystalline domain;

- Crystalline mixture: identification of the crystalline phases and quantitative determination of their weight fractions;

- Nanoscale assembly: positions/symmetry of the nanoparticles/nanocrystals in the assembly and extension of the assembly.

3.3 Field emission scanning electron microscopy (FESEM)

The electron microscope works as a light microscope. However, electron microscope can differ because of the wavelength. The electron microscope has very energetic electrons that have a very short wavelength compared to optical microscope. That is why electron microscope is very effective to observe nanoparticles. The wavelength of the electron microscope can be written as:

$$\lambda = \sqrt{\frac{1.5}{V\left(1 + V * 10^{-6}\right)}} nm$$

The extremely small wavelength makes it possible to show the structure of nanoparticles by FESEM.FESEM uses Field Emission Gun producing a cleaner image. It has also some advantages over SEM test, those are it shows less electrostatic distortions and good resolution< 2nm.

3.4 UV visible spectroscopy

Ultraviolet/Visible/Infrared (UV/Vis/IR) spectroscopy is the technique by which we measure the attenuation of light that is scattered and absorbed by a sample (absorption+ scattering= excitation). UV visible is a vital technique to identify, characterize and study specific nanoparticle. The wavelength of ultraviolet is 200-400nm and visible is 400-800nm. It follows the Beer lambert law:

$$A=\log (I_O/I)=Ecl$$

Here, the absorption of the light is directly proportional to concentration(c) and path length (l). The most common applications of UV visible technique aredetection of Chromophore functional group, determine the unknown compound, purity of the sample, bandgap calculations, etc. [87].

3.5 Fluorescence spectroscopy

In-room temperature, all the molecules remain in ground state. The ground state is the lowest energy level of the molecules. Within the ground states are vibrational levels, which is the lowest vibrational state. When the molecules excite, they go into highest energy level. Then the molecules absorb particular wavelength of light. However, for the collision with other molecules, they return in the ground state. In the ground state, they emit certain wavelengths of light that are different from the absorbed light. The emission of light is fluorescence. The emission and excitation spectrum indicate the change of sample. The change of wavelength and peak is caused by normal temperature, concentration, and collision with other molecules.

3.6 Fluorescence microscopy

"Fluorescence microscope" refers to any microscope that uses fluorescence to generate an image, whether it is a more simple set up like an epifluorescence microscope or a more complicated design such as a confocal microscope, which uses optical sectioning to get better resolution of the fluorescence image. Fluorescence microscopy is widely using in biology, biomedical science and material science. By fluorescence microscopy, it is able to detect the single-molecule in particles. It made it possible to identify cells and sub-microscopic cellular components because of having higher degree of specificity. The basic fundamental of it is to expose light to specific sample and to separate the weaker fluorescence from the excitation light [88].

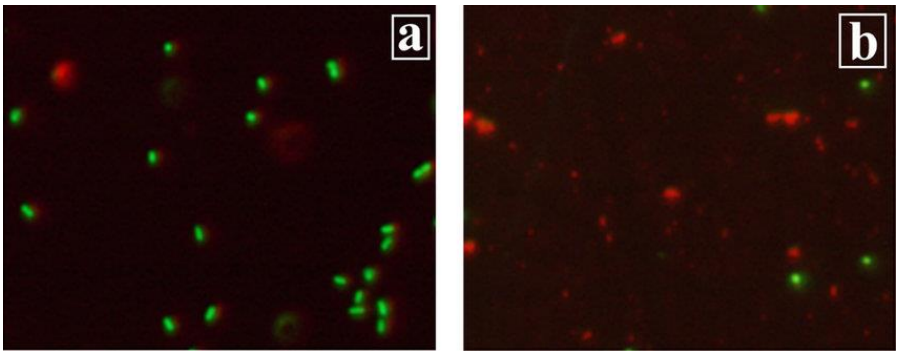

Figure- 3.1: Comparison of bacteria treated with of silver nanoparticles with control bacteria (treated with phosphate-buffered saline) as visualized by fluorescence microscopy after staining with Live/Dead Bac Light reagent, (a) intact bacteria structure; (b) damaged bacteria structure[89]

3.7 Zeta potential

Zeta potential is a proportion of the viable electric charge on the nanoparticle surface in solution (colloids). The greatness of the zeta potential gives data about molecule stability, with particles with higher extent zeta possibilities displaying higher stability because of a bigger electrostatic repulsion between particles. By the surface charge of nanoparticles in the slipping plane, it is easy to determine the state of electric charge on the surface and to predict the stability of nanoparticle, which helps to characterize the nanoparticles, as seen in the equation [90].

$$Q = 4\pi\varepsilon\varepsilon_o\zeta r(1 + \kappa r)$$

The surface charge of the nanoparticles attracts thin layer of opposite charge. This double layer ions move in the solution. The electric potential difference at the boundary of the two layers is called zeta potential. The range of zeta potential normally from +100mV to -100 and +25 mV to -25mV is considered as higher value.

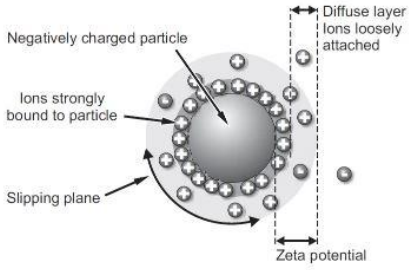

Figure-3.2: Zeta potential measurement

3.8 Atomic absorption spectroscopy (AAS)

Atomic absorption spectrometry (AAS) is an analytical technique that measures the concentrations of elements. Particles have valence electrons, which are the peripheral electrons of the molecule. Molecules can be energized when lighted. At the point when a particle is energized, the valence electron climbs a vitality level. The energies of the different stationary states, or limited circles, would then be able to be dictated by these emanation lines. The reverberation line is then characterized as the particular radiation assimilated to arrive at the energized states; this is the main theory of this technique [91]. AAS is a commonly used technique for the determination of single elements in compounds. AAS of different materials can be compared by the absorption vs time graph.

3.9 Fourier-transform infrared spectroscopy (FTIR)

Fourier-transform infrared spectroscopy (FTIR)is a technique used to obtain an infrared range of absorption or emission of a solid, liquid or gas. Infrared spectrometer measures the infrared radiation of gradual increasing wavelength moves through the sample and percentage of transmittance. The percentage of transmittance vs wavenumber (cm^{-1}) graph is called an infrared spectrum. The molecules do not vibrate at room temperature. When the molecule absorbs light and energy, they excite and start vibrating. Such absorption can occur only if there is difference in the two vibrational levels of the dipole moment of the molecule[92].

3.10 Conclusion

To sum up, though there are several numbers of techniques, the above-mentioned techniques are well known and reliable to detect the property of nanomaterial. Some techniques identify stability, some observe a variety of vibration, some give microscopy view, etc. By the analysis of the result, we can have a clear idea about shapes, size, and property of nanomaterial, which helps to characterize it.

Chapter 4

Experimental result analysis and characterization of nanomaterials

4.1 Introduction

In the experimental part, we characterize some water samples from different sources by some of the techniques mentioned in chapter 3. This section covers the result analysis of **pH. Fourier-transform infrared spectroscopy (FTIR), Atomic Absorption Spectroscopy (AAS) and Fluorescence spectroscopy** test with necessary graphs and images. It will reflect the properties of treated and untreated of different water samples. There are many different sources of wastewater in Bangladesh. We can use the waste or drinking water in our daily activities if they are not harmful for the soil, insects, animals and so on. Hence, we need to know the elements in the wastewater. If they are in safe range then we can easily reuse the water agriculture, washing etc. We choose pH test that indicates whether the water is base, acidic or neutral, FTIR test shows the carbon and hydrogen bonding in samples, AAS test gives the concentration of metals in samples and fluorescence spectroscopy test shows emission and excitation spectrum. By all the values and graphs, we can easily get an idea whether the water sample is safe for the environment or not.

4.2 Water samples from different sources

For the characterization of water, we collect different sources of waters including waste and drinking from different locations in Bangladesh. The samples are-

i. The treated garments wastewater is from Narayanganj area, where most of the garments factories are situated.
ii. Pharmaceutical wastewater is also from Narayanganj and it is ETP (Effluent Treatment Plant) discharged.
iii. The lake water is from the Gulshan area.
iv. The tap water from Brac University.
v. The untreated garments water (Direct washing water from a common source of American Eagle, Levis, Uniqlo, H&M garments)

(i)

(ii)

(iii)

(iv)

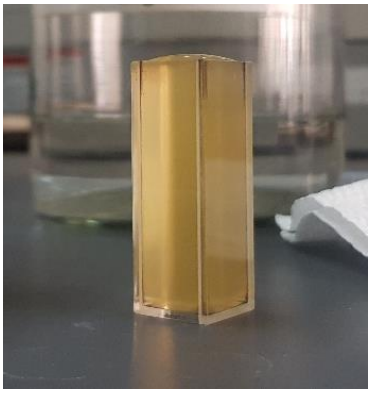

(v)

Figure-4.1: Sample of (i) garments wastewater, (ii) pharmaceutical wastewater, (iii) lake water, (iv) tap water and (v) untreated garments water

4.3 Experimental characterization and result analysis

In this part, we will analysis our experimental results with the reference value, so that we can characterize our samples. We did pH analysis, FTIR analysis to see the bonding of different molecules, AAS for observing the concentration of element in our samples and fluorescence for measuring the intensity of elements.

4.3.1 pH experimental result analysis

pH stands for the 'potential of hydrogen'. By pH value, it can be identified whether the water-soluble is acidic or alkaline. The acidity or alkalinity of wastewater is harmful to both wastewater treatment and the environment. Low pH is acidic, high pH is alkaline, and pH of 7 is neutral. In our experimental part, we also tried to analyze pH values for the different sources of water, as mentioned earlier, in order to treatment.

Sample	Parameters	Concentration
1. Garments wastewater (after treatment)	pH at 25.2^0 C	7.55
2. Pharmaceutical wastewater (after treatment)	pH at 25.1^0 C	7.30
3. Tap water	pH at 24.8^0 C	7.21
4. Lake water	pH at 25.1^0 C	6.65

Table-4.1: Sample of water from different sources with their pH value

From the table-4.1, we can analyze the pH values from different sources of water. The pH values are above 7, which is basically shows the properties of basic, as mentioned before. Therefore, the result that we got from the experiment is matched with the standard value.

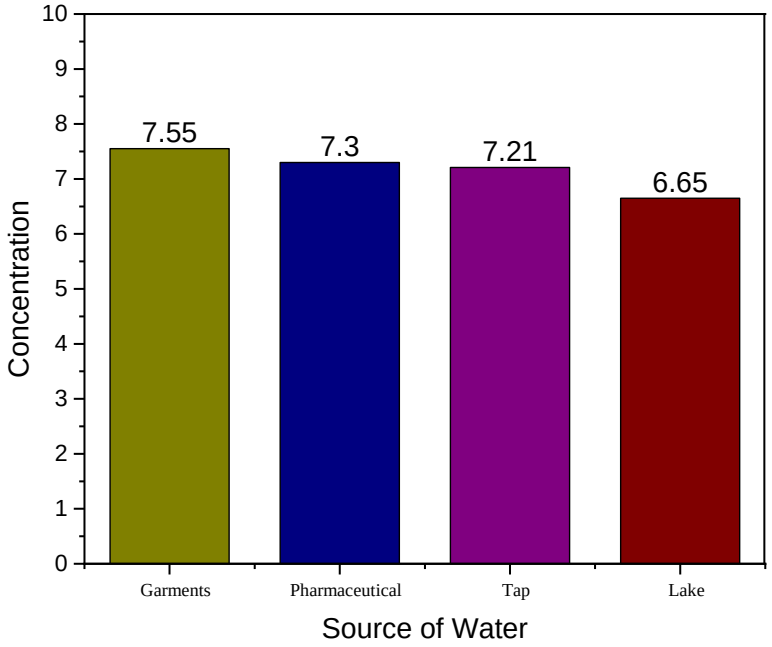

Figure-4.2: Bar chart of pH variation

Garments wastewater has a harmful impact on the environment because the effluent is mixed up with various contaminates. So, the factories treat the water before they discharge it. The experimental value is after the treatment of water. The garments are mainly produced synthetic fabrics. In fiber production there is a wet process that mainly discharges high contamination of water. This process consists of sizing, de-sizing, sourcing, bleaching, dyeing, printing and finishing techniques. According to a review paper the effluents of dye industry has high pH [93]. Another study [94] also shows that most of the garments factory has alkaline characteristics because there are many alkaline elements. Our experimental result also shows the properties of alkaline having pH 7.55.

The pharmaceutical wastewater that we used for our experiment is ETP (Effluent Treatment Plant) water. The pH value is 7.3 which is above the neutral value of pH range. The company produced a variety type of medicines that generates contaminated water. Some research shows that the pH parameter of discharge water from different pharmaceutical companies. They indicate that normally the standard they consider which ranges 6-8.5. The pharmaceutical wastewater has some parameter phosphate, sulphides, phenolics, lead, chromium, etc., which makes the water base. These parameters can vary from industry to industry[95].

We collected the tap water from Brac University. The pH 7.21 value is close to the neutral value of the range. According to HealthLine typically the tap water is considered 7.5. So, we can consider the value is satisfying.

Gulshan lake water is considered a critical level of contaminated water because of heavy pollutants. Untreated sewage, direct dumping solids, industrial waste, chemicals, etc. are mainly responsible for the pollution. The pH is 6.65 which shows acidic properties. The pH is harmful to the aquatic organism.

4.3.2 Fourier-transform infrared spectroscopy (FTIR) experimental result analysis

For identifying the unknown materials, amount of component mixed in the sample and quality of a sample, we did FTIR experiment. In FTIR test IR (Infrared Ray) radiation pass through the sample. The sample absorbs or transmits the rays. As we discussed earlier, all the material has different atomic structure, so the infrared spectrum is also different. In our experiment part, we choose two samples. One is i) Garments wastewater and ii) Tap water.

In Table-4.2 and Table-4.3 are shown our experimental data with analysis using IR peak analysis table [96] and relevant paper[97], which is showing different types of bonding.

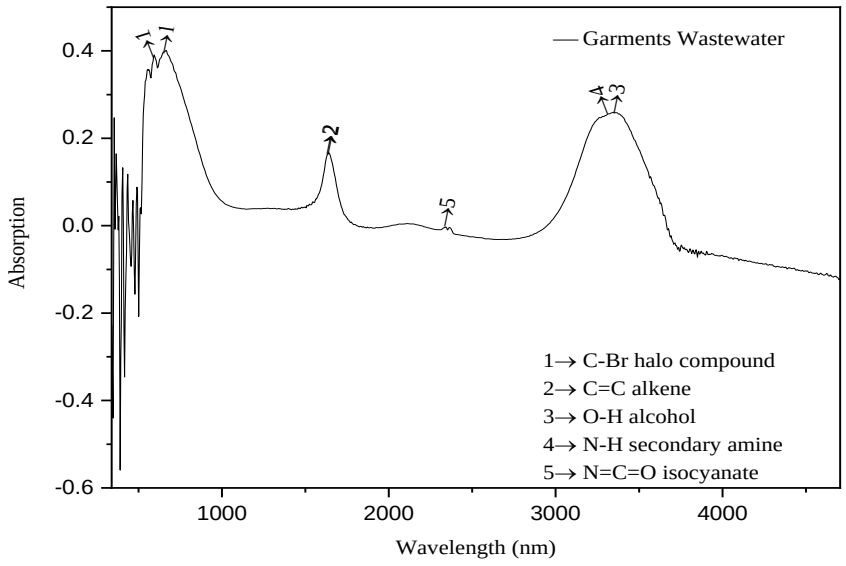

(i)

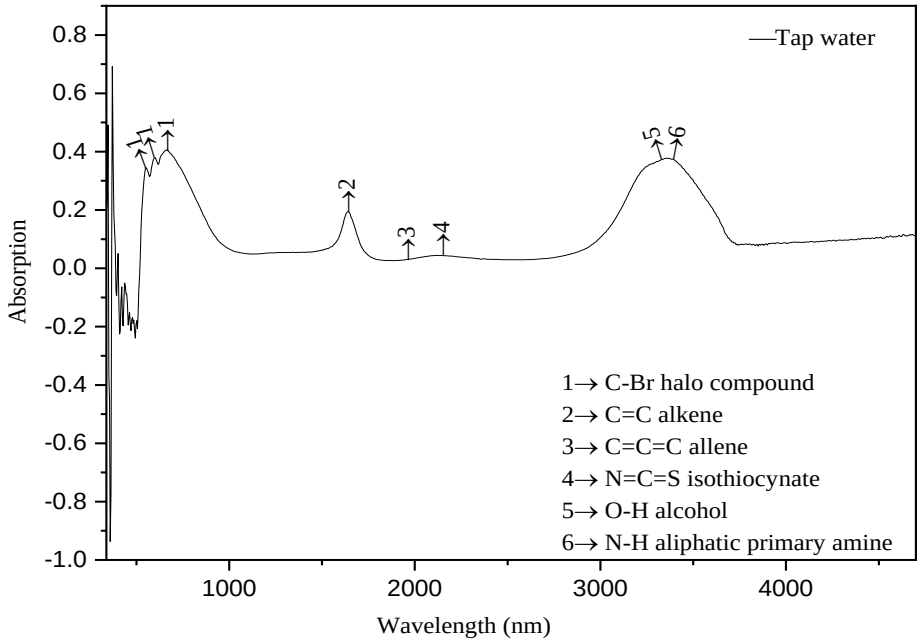

(ii)

Figure-4.3: FTIR graph absorption vs wavelength (nm) for (i) garments wastewater and (ii) tap water

Absorption peak (cm^{-1})	**Functional group**	**Type of vibration**	**Intensity**
3263.56	O-H alcohol & N-H secondary amine	Stretch	Strong, broad
3313.71	O-H alcohol & N-H secondary amine	Stretch	Strong, broad
3344.57	O-H alcohol & N-H secondary amine	Stretch	Medium
3360.00	O-H alcohol & N-H secondary amine	Stretch	Medium
1639.49	C=C alkene	Stretch	Medium
1400.32	C-H aldehyde	Bend	Strong
1273.02	C-O alkyl aryl ether	Stretch	Strong
1249.87	C-O alkyl aryl ether	Stretch	Strong
1222.87	C-N amine	Stretch	Medium
1184.29	C-O ester	Stretch	Strong
1639.49	C=C alkene	Stretch	Medium
3360.00	O-H alcohol & N-H aliphatic primary amine	Stretch	Medium

3344.00	O-H alcohol & N-H aliphatic primary amine	Stretch	Medium

Table-4.2: Fourier transform infrared spectroscopy absorption table for garments wastewater [96, 97]

Absorption peak (cm^{-1})	**Functional group**	**Type of vibration**	**Intensity**
4000.36	O-H alcohol	Sharp	Medium
3803.63	O-H alcohol	Sharp	Medium
3348.42	N-H aliphatic primary amine	Stretch	Medium
3278.99	O-H alcohol	Stretch	Strong
2692.63	C-H aldehyde	Stretch	Medium
2665.62	C-H aldehyde	Stretch	Medium
2106.27	N=C=S isothiocyanate	Stretch	Strong
1913.39	C=C=C allene	Stretch	Mediun
1870.95	C-H aromatic compound	Bending	Weak
1639.49	C=C alkene	Stretch	Medium
1300.02	C-O aromatic ester	Stretch	Strong
1273.02	C-O alkyl aryl ether	Stretch	Strong
1215.15	C-O venyl ether	Stretch	Strong
1188.15	S=O sulfonate	Stretch	Strong
601.79	C-Br halo compound	Stretch	Strong
551.64	C-Br halo compound	Stretch	Strong

Table-4.3: Fourier transform infrared spectroscopy absorption table for tap water[96]

From the table-4.2 and table-4.3 we get the data of different types of bonding that present in the two samples. We can predict the elements present in these samples. In the garments water carbon, hydrogen, nitrogen, sulphare, oxide, fluoride etc. are present. In tap water we also observe the variety of elements like sulphare, boron, etc. We also get some compounds; they are halo compound, aromatic compound. Therefore, from the FTIR test, we get the idea about the components in these two types of water samples.

4.3.3 Atomic Absorption Spectroscopy (AAS) experimental result analysis

AAS is a popular technique to detect metal and metalloids in samples. It is a very reliable and simple method to use. It also determines the concentration of metals by using the wavelength of ultraviolet or visible light that the element absorbs. Atomic absorption spectroscopy quantifies the absorption of ground-state atoms in the gaseous state.

In our experimental analysis, for determining the concentration of metal, we use the untreated garments wastewater (v). We observed the concentration of three harmful metals, which are Chromium (Cr), Lead (Pb) and Silver (Ag). The methodology/ instrument is APHA method (Atomic Absorption Spectrometer).

Parameters	Concentration (ppm)	Safe range
Chromium (Cr)	~ 0.10	US EPA= 0.10mg/L WHO= 0.05mg/L
Lead (Pb)	~ 0.20	US EPA= 0.015mg/L WHO= 0.01mg/L
Silver (Ag)	~ 0.10	US EPA= 0.10mg/L WHO= 0.10mg/L

Table-4.4: Atomic Absorption Spectroscopy (AAS) table for untreated garments wastewater

The maximum contamination level (MCL) actually indicates the value of safe range of water. MCL is the highest level of a contaminant that is allowed in drinking water. According to US EPA (United States Environmental Protection Agency) the MCL of Cr is in the water is 0.10mg/L (ppm). The WHO (World Health Organization) sets the value 0.05mg/L (ppm). The California MCL also tells the safe range is 0.05mg/L of Cr [98]. Considering our experimental value it is not in the safe range. Moreover, according to US EPA the safe range of lead is 0.015mg/L and also WHO says the safe range is 0.10 mg/L[99]. Again, the safe range for silver element in water is 0.1 mg/L, according to the US EPA and WHO [100]. To conclude the result, the experimental result of lead and silver that we got are not safe.

We experimented for a single water sample. If we want to get more accurate value, then more samples from different sources needs to be tested. In future we will extend the experiment.

4.3.4 Fluorescence experimental result analysis

All our fluorescence studies were performed using the Hitachi F-7000 Fluorescence Spectrophotometer with a properly corrected background. Fluorescence spectra were obtained by using a xenon beam of having wavelength of 300nm to 700nm and due to fluorescence properties our samples absorb light at one wavelength and then reemitting it another wavelength [101]. In our experimental analysis, we use the untreated garments wastewater.

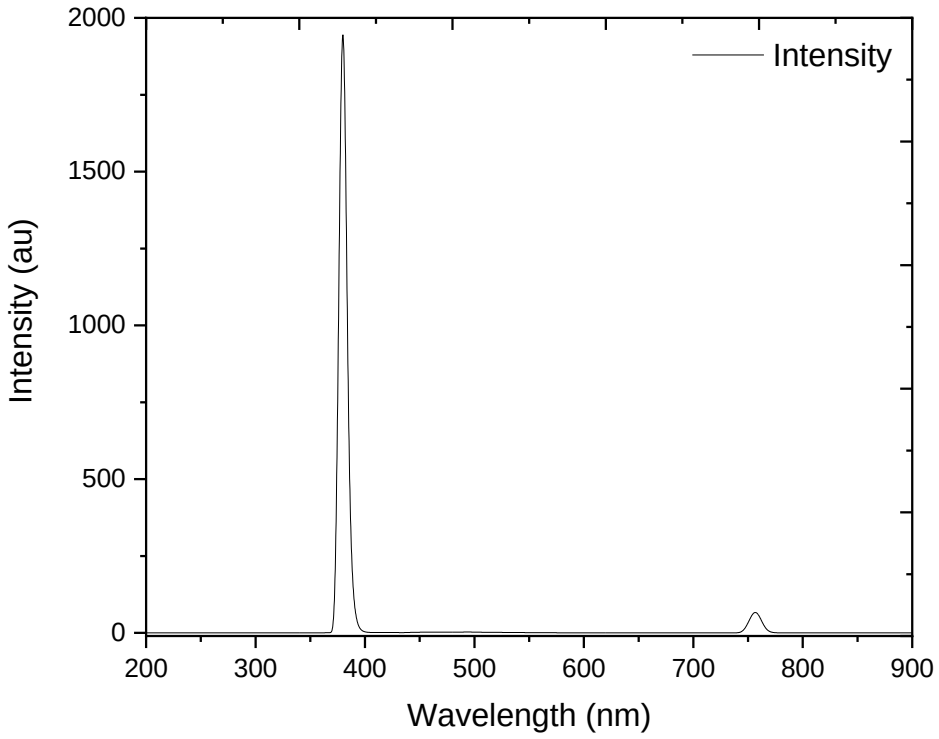

(i)

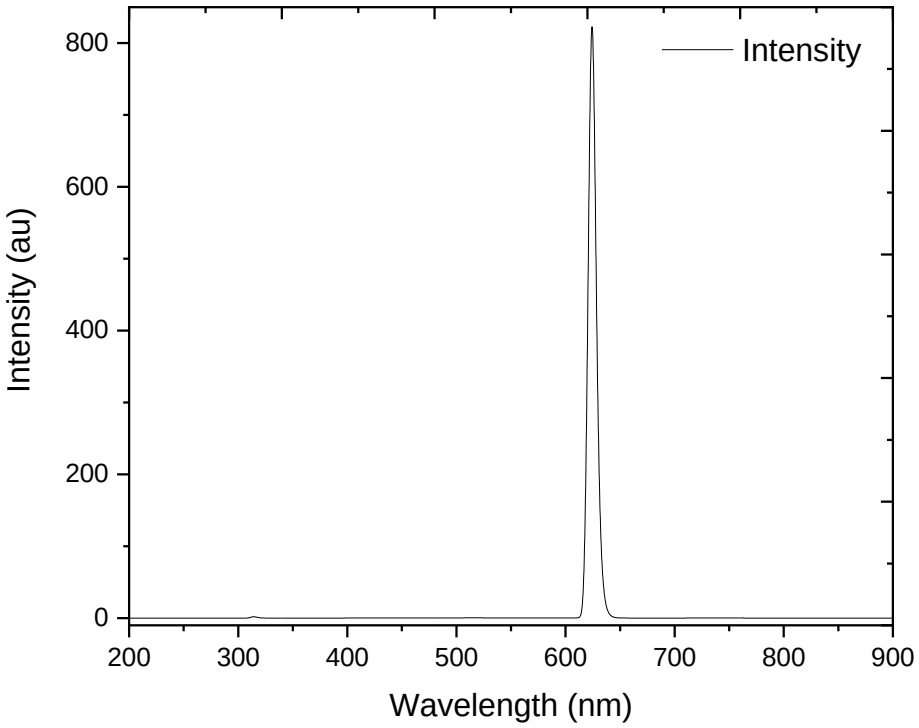

(ii)

Figure-4.4: (i)Fluorescence intensity vs wavelength at excitation of 375 nm and (ii)620 nm for untreated garments wastewater

Here, we can observe that fluorescence intensity is stronger around 375 nm in figure-4.4(i) which is wavelength of silver nano particle and the small peak that can be silver coupling, its need to do further analysis to determine it. In addition, in figure 4.4(ii), the stronger intensity is around 625 nm, which is wavelength of gold nano particle, or it can be another particle as well. The intensity is much stronger in figure-4.4(i) which is about 1950 au and that suggests us that the concentration of silver is high in the sample.

Chapter 5
Conclusion

5.1 Thesis Conclusion

Our research study has described the characterization of plasmonic nanoparticle properties. In our research, we explored a significant property to develop a convenient tool for wastewater purification.

In our systematic analysis, we did a literature review on the water treatment system by plasmonic nanoparticle and also addressed some applications of plasmonic nanoparticle. We also mentioned various optical properties of nanomaterial. Using Mie theory, we did analytical simulation for single gold nanoparticle. We used FDTD numerical simulation tool for the characterization of silver nanoparticle by observing absorption, scattering and extinction characteristics.

We also did some experimental analysis for the qualitative and quantitative analysis of our water samples from different sources. pH experiment has been used to determine the nature of the sample, whether they are acidic or alkaline. Moreover, by using AAS method, we got the concentration of harmful elements such as Pb, Cr, and Ag in the wastewater sample. The concentration range of these elements is out of safe range which refers that using this water is highly hazardous to our health. Additionally, FTIR and Fluorescence Spectroscopy have been used to determine the chemical bonding and verify the present of plasmonic nanoparticle in several sources water sample. This experimental analysis is just for a few water samples, but for getting better and accurate results, various analyses on different water samples, need to be done

To conclude, our motivation of thesis research is to identify the optical characteristics and applied them for wastewater treatment to meet up the water scarcity problem in Bangladesh.

5.2 Future work

For a large populated country, water purification is quiet challenging matter. Therefore, our research study can be extended to solve the major problem of water pollution in Bangladesh. In future we will extend our works which includes-

1. This work is just a preliminary stage that shows the presence and concentration of some harmful molecules like lead, silver and chromium. In future, we want to identify some other harmful molecules in the sample, so that we can remove them and can use the water in our daily activities [74].

2. Our focus is not only on plasmonic material, but also, we want to determine all kind of nanomaterials, so that we can reuse the wastewater and drinking water. So, our water crisis can be met up in future.

3. We will also do some microscopic experiments like FESEM, for a better understanding about the sample, which will help us for further analysis to reach our goal.

4. Some other reliable methodologies like Zeta potential, XRD and ICP-MS will be done in future. By using these significant methods, we can appropriately quantify the number of harmful particles in water.

We believe that our qualitative and quantitative analysis in water samples will be effective in future to remove water scarcity from Bangladesh.

References:

1. Eustis, S. and M.A.J.C.s.r. El-Sayed, *Why gold nanoparticles are more precious than pretty gold: noble metal surface plasmon resonance and its enhancement of the radiative and nonradiative properties of nanocrystals of different shapes*. 2006. **35**(3): p. 209-217.
2. Yu, Peng & Yao, Yisen & Wu, Jiang & Niu, Xiaobin & Rogach, Andrey & Wang, Zhiming, *Effects of plasmonic metal core-dielectric shell nanoparticles on the broadband light absorption enhancement in thin film solar cells.* 2017. **7**(1): p. 7696.
3. Shuwen Zeng, Xia Yu, Wing-Cheung Law, Yating Zhang, Rui Hu, Xuan-Quyen Dinh, Ho-Pui Ho, Ken-Tye Yong, *Size dependence of Au NP-enhanced surface plasmon resonance based on differential phase measurement.* 2013. **176**: p. 1128-1133.
4. Jiang Wu, Peng Yu, Andrei S. Susha, Kimberly A. Sablon, Haiyuan Chen, Zhihua Zhou, Handong Li, Haining Ji, Xiaobin Niu, Alexander O. Govorov, Andrey L. Rogach, Zhiming M. Wang, *Broadband efficiency enhancement in quantum dot solar cells coupled with multispiked plasmonic nanostars.* 2015. **13**: p. 827-835.
5. de Aberasturi, D.J., A.B. Serrano-Montes, and L.M.J.A.O.M. Liz-Marzán, *Modern applications of plasmonic nanoparticles: from energy to health.* 2015. **3**(5): p. 602-617.
6. Ming Hua, Shujuan Zhang, Bingcai Pan, Weiming Zhang, Lu Lv, Quanxing Zhang, *Heavy metal removal from water/wastewater by nanosized metal oxides: a review.* 2012. **211**: p. 317-331.
7. Grossl, Paul & Sparks, Donald & Ainsworth, Calvin, *Rapid kinetics of Cu (II) adsorption/desorption on goethite.* 1994. **28**(8): p. 1422-1429.
8. Chen, Y.-H., F.-A.J.J.o.C. Li, and I. Science, *Kinetic study on removal of copper (II) using goethite and hematite nano-photocatalysts.* 2010. **347**(2): p. 277-281.
9. Dantas, T.D.C., A.D. Neto, and M.D.A.J.W.R. Moura, *Removal of chromium from aqueous solutions by diatomite treated with microemulsion.* 2001. **35**(9): p. 2219-2224.
10. C.H. Weng, J.H. Wang, C.P. Huang, *Adsorption of Cr (VI) onto TiO2 from dilute aqueous solutions.* 1997. **35**(7): p. 55-62.

11. Babel, S. and T.A.J.C. Kurniawan, *Cr (VI) removal from synthetic wastewater using coconut shell charcoal and commercial activated carbon modified with oxidizing agents and/or chitosan.* 2004. **54**(7): p. 951-967.
12. Ming Fan, Thipnakarin Boonfueng, Ying Xu, Lisa Axe, Trevor A. Tyson, *Modeling Pb sorption to microporous amorphous oxides as discrete particles and coatings.* 2005. **281**(1): p. 39-48.
13. Engates, K.E., H.J.J.E.S. Shipley, and P. Research, *Adsorption of Pb, Cd, Cu, Zn, and Ni to titanium dioxide nanoparticles: effect of particle size, solid concentration, and exhaustion.* 2011. **18**(3): p. 386-395.
14. Liang, Pei & Shi, Taqing & Li, Jing, *Nanometer-size titanium dioxide separation/preconcentration and FAAS determination of trace Zn and Cd in water sample.* 2004. **84**(4): p. 315-321.
15. Moses, V., *Nanotechnology-As antibacterial and heavy metal removal in waste water treatment-A review Nanotechnology-As Antibacterial and Heavy Metal Removal In Waste Water Treatment-A Review*. 2018.
16. Tiwari, D.K., J. Behari, and P. Sen, *Application of nanoparticles in waste water treatment 1.* 2008.
17. Ottaviani, Maria & Favuzza, Paolo & Bigazzi,, Massimo & Turro, Nicholas & Jockusch, Steffen & Tomalia, Donald, *A TEM and EPR investigation of the competitive binding of uranyl ions to starburst dendrimers and liposomes: Potential use of dendrimers as uranyl ion sponges.* 2000. **16**(19): p. 7368-7372.
18. Arkas, M., D. Tsiourvas, and C.M.J.C.o.m. Paleos, *Functional dendrimeric "nanosponges" for the removal of polycyclic aromatic hydrocarbons from water.* 2003. **15**(14): p. 2844-2847.
19. Marambio-Jones, C. and E.M.J.J.o.N.R. Hoek, *A review of the antibacterial effects of silver nanomaterials and potential implications for human health and the environment.* 2010. **12**(5): p. 1531-1551.
20. Praveena, S.M., A.Z.J.W.Q. Aris, Exposure, and Health, *Application of low-cost materials coated with silver nanoparticle as water filter in Escherichia coli removal.* 2015. **7**(4): p. 617-625.
21. Heidarpour, Farideh & Ghani, Wan & Fakhru'l-Razi, A. & Sobri, Shafreeza & Heydarpour, V. & Zargar, Mohsen & Mozafari, *Complete removal of pathogenic bacteria from drinking water using nano silver-coated cylindrical polypropylene filters.* 2011. **13**(3): p. 499-507.

22. Rai, M., A. Yadav, and A.J.B.a. Gade, *Silver nanoparticles as a new generation of antimicrobials.* 2009. **27**(1): p. 76-83.
23. Feng, Qing & Wu, J. & Chen, Guo-Qiang & Cui, Fu-Zhai & Kim, T. & Kim, *A mechanistic study of the antibacterial effect of silver ions on Escherichia coli and Staphylococcus aureus.* 2000. **52**(4): p. 662-668.
24. Brown, Joe, *Effectiveness of ceramic filtration for drinking water treatment in Cambodia.* 2008.
25. Su, Hong-Lin & Lin, Siou-Hong & Wei, Jiun-Chiou & Pao, I-Chuan & Chiao, Shu-Her & Huang, Chieh-Chen & Lin, Shinn-Zong & Lin, Jiang-Jen, *Novel nanohybrids of silver particles on clay platelets for inhibiting silver-resistant bacteria.* 2011. **6**(6): p. e21125.
26. Kaufman, Y. and V. Freger, *Supported biomimetic membranes for pressure-driven water purification*, in *On Biomimetics*. 2011, IntechOpen.
27. Han, Y., Z. Xu, and C.J.A.F.M. Gao, *Ultrathin graphene nanofiltration membrane for water purification.* 2013. **23**(29): p. 3693-3700.
28. Weiwei He, Ying Liu, Jinshan Yuan, Jun-Jie Yin, Xiaochun Wu, Xiaona Hu, Ke Zhang, Jianbo Liu, Chunying Chen, Yinglu Ji, Yuting Guo, *Au@ Pt nanostructures as oxidase and peroxidase mimetics for use in immunoassays.* 2011. **32**(4): p. 1139-1147.
29. Runping Han, Dandan Ding, Yanfang Xu, Weihua Zou, Yuanfeng Wang, Yufei Li, Lina Zou, *Use of rice husk for the adsorption of congo red from aqueous solution in column mode.* 2008. **99**(8): p. 2938-2946.
30. Afkhami, A. and R.J.J.o.H.M. Moosavi, *Adsorptive removal of Congo red, a carcinogenic textile dye, from aqueous solutions by maghemite nanoparticles.* 2010. **174**(1-3): p. 398-403.
31. Yu, Chichao & Dong, Xiaoping & Guo, Limin & Li, Jiangtian & Qin, Fei & Zhang, Lingxia & Shi, Jianlin & Yan, Dongsheng, *Template-free preparation of mesoporous Fe2O3 and its application as absorbents.* 2008. **112**(35): p. 13378-13382.
32. Dadvar, Elahe & Rezaei Kalantary, Roshanak & Panahi, Homayon & Peyravi, Majid, *Efficiency of polymeric membrane graphene oxide-TiO2 for removal of azo dye.* 2017. **2017**.
33. Mohsin, A.J.M.S.U.o.T., *Aggregation and uptake kinetics of gold nanoparticles in biological cells, using plasmon coupling and image correlation spectroscopy [PhD thesis]*. 2015.

34. Sokolov, Konstantin & Follen, Michele & Aaron, Joann & Pavlova, Ina & Malpica, Anais & Lotan, Reuben & Kortum, Rebecca, *Real-time vital optical imaging of precancer using anti-epidermal growth factor receptor antibodies conjugated to gold nanoparticles.* 2003. **63**(9): p. 1999-2004.
35. Jiang & Gu, Hongwei & Shao, Huilin & Devlin, Eamonn & Papaefthymiou, Georgia & Ying, Jackie., *Bifunctional Fe3O4–Ag heterodimer nanoparticles for two-photon fluorescence imaging and magnetic manipulation.* 2008. **20**(23): p. 4403-4407.
36. Sotiriou, G.A.J.W.I.R.N. and Nanobiotechnology, *Biomedical applications of multifunctional plasmonic nanoparticles.* 2013. **5**(1): p. 19-30.
37. Aaron, Joann & Travis, Kort & Harrison, Nathan & Sokolov, Konstantin, *Dynamic imaging of molecular assemblies in live cells based on nanoparticle plasmon resonance coupling.* 2009. **9**(10): p. 3612-3618.
38. El-Sayed, I.H., X. Huang, and M.A.J.N.l. El-Sayed, *Surface plasmon resonance scattering and absorption of anti-EGFR antibody conjugated gold nanoparticles in cancer diagnostics: applications in oral cancer.* 2005. **5**(5): p. 829-834.
39. Goyal, R.N., S. Chatterjee, and A.R.S.J.C. Rana, *The effect of modifying an edge-plane pyrolytic graphite electrode with single-wall carbon nanotubes on its use for sensing diclofenac.* 2010. **48**(14): p. 4136-4144.
40. Revin, S.B. and S.A.J.A. John, *Electrochemical sensor for neurotransmitters at physiological pH using a heterocyclic conducting polymer modified electrode.* 2012. **137**(1): p. 209-215.
41. Chen, A. and S.J.C.S.R. Chatterjee, *Nanomaterials based electrochemical sensors for biomedical applications.* 2013. **42**(12): p. 5425-5438.
42. Lei, J., H.J.W.I.R.N. Ju, and Nanobiotechnology, *Nanotubes in biosensing.* 2010. **2**(5): p. 496-509.
43. Wu, L., X. Zhang, and H.J.A.c. Ju, *Detection of NADH and ethanol based on catalytic activity of soluble carbon nanofiber with low overpotential.* 2007. **79**(2): p. 453-458.
44. Wu, S., H. Ju, and Y.J.A.F.M. Liu, *Conductive mesocellular silica–carbon nanocomposite foams for immobilization, direct electrochemistry, and biosensing of proteins.* 2007. **17**(4): p. 585-592.
45. Shi, Lihong & Liu, Xiaoqing & Niu, Wenxin & Li, Haijuan & Han, Shuang & Chen, Jiuan & Xu, Guobao, *Hydrogen peroxide biosensor based on direct electrochemistry of soybean peroxidase immobilized on single-walled carbon nanohorn modified electrode.* 2009. **24**(5): p. 1159-1163.

46. Tang, Yifan & Allen, Brett & Kauffman, Douglas & Star, Alexander, *Electrocatalytic activity of nitrogen-doped carbon nanotube cups.* 2009. **131**(37): p. 13200-13201.
47. Xu, Xuan & Jiang, Shujuan & Hu, Zheng & Liu, Songqin, *Nitrogen-doped carbon nanotubes: high electrocatalytic activity toward the oxidation of hydrogen peroxide and its application for biosensing.* 2010. **4**(7): p. 4292-4298.
48. Haes, A.J., R.P.J.A. Van Duyne, and b. chemistry, *A unified view of propagating and localized surface plasmon resonance biosensors.* 2004. **379**(7-8): p. 920-930.
49. Kumar, S. and S. Tanwar, *Nanoantenna - A Review on Present and future Perspective.* International Journal of Science Engineering & Technology, 2016. **4**: p. 240-247.
50. Kreibig, U. and M. Vollmer, *Optical properties of metal clusters*. Vol. 25. 2013: Springer Science & Business Media.
51. Hergert, W. and T. Wriedt, *The Mie theory: basics and applications*. Vol. 169. 2012: Springer.
52. Luo, X., J. Ma, and T. Ishihara, *Plasmon-related optical properties of unpenetrated metallic periodic structures.* Optical Materials, 2006. **29**(2): p. 211-215.
53. Johnson, P.B. and R.W. Christy, *Optical Constants of the Noble Metals.* Physical Review B, 1972. **6**(12): p. 4370-4379.
54. Mohsin, Asm, *Aggregation and Uptake Kinetics of Gold Nanoparticles in Biological Cells, Using Plasmon Coupling and Image Correlation Spectroscopy*. 2015.
55. May Hlaing, Bellsabel Gebear-Eigzabher, Azael Roa, Aristides Marcano, Daniela Radu, Cheng-Yu Lai, *Absorption and scattering cross-section extinction values of silver nanoparticles.* Optical Materials, 2016. **58**: p. 439-444.
56. Fu, Q. and W. Sun, *Mie theory for light scattering by a spherical particle in an absorbing medium.* Applied Optics, 2001. **40**(9): p. 1354-1361.
57. Wriedt, T., *Mie theory: a review*, in *The Mie Theory*. 2012, Springer. p. 53-71.
58. Gutierrez Villarreal, J.M., J.A. Gaspar Armenta, and L.A. Mayoral Astorga, *Surface plasmon field enhancement: excitation by a short pulse or narrow beam of light.* Journal of the Optical Society of America B, 2018. **35**(5): p. 1040-1045.
59. A.S. Shalin, S.V. Sukhov, A.E. Krasnok, S.A. Nikitov, *Plasmonic nanostructures for local field enhancement in the UV region.* Photonics and Nanostructures - Fundamentals and Applications, 2014. **12**(1): p. 2-8.
60. Coronado, E., E. Encina, and F. Stefani, *Optical properties of metallic nanoparticles: Manipulating light, heat and forces at the nanoscale.* Nanoscale, 2011. **3**: p. 4042-59.

61. Mondes, Valerie & Antonsson, Egill & Plenge, Jürgen & Raschpichler, C. & Halfpap, I. & Menski, Antonia & Graf, Christina & Kling, Matthias & Rühl, E., *Plasmonic electric near-field enhancement in self-organized gold nanoparticles in macroscopic arrays.* Applied Physics B, 2016. **122**.
62. Khlebtsov, N.G. and L.A. Dykman, *Optical properties and biomedical applications of plasmonic nanoparticles.* Journal of Quantitative Spectroscopy and Radiative Transfer, 2010. **111**(1): p. 1-35.
63. Hutter, E. and J.H. Fendler, *Exploitation of localized surface plasmon resonance.* Advanced materials, 2004. **16**(19): p. 1685-1706.
64. Jain, P.K., Huang, X., El-Sayed, I.H., & El-Sayed, M.A., *Review of Some Interesting Surface Plasmon Resonance-enhanced Properties of Noble Metal Nanoparticles and Their Applications to Biosystems.* Plasmonics, 2007. **2**(3): p. 107-118.
65. Amendola, Vincenzo & Pilot, Roberto & Frasconi, Marco & Marago, Onofrio M. & Iatì, Maria, *Surface plasmon resonance in gold nanoparticles: a review.* Journal of Physics: Condensed Matter, 2017. **29**(20): p. 203002.
66. Khan, I., K. Saeed, and I. Khan, *Nanoparticles: Properties, applications and toxicities.* Arabian Journal of Chemistry, 2017.
67. Nehl, Colleen & Grady, Nathaniel & Goodrich, Glenn & Tam, Felicia & Halas, Naomi & Hafner, Jason, *Scattering Spectra of Single Gold Nanoshells.* Nano Letters, 2004. **4**(12): p. 2355-2359.
68. Cox, A., A.J. DeWeerd, and J. Linden, *An experiment to measure Mie and Rayleigh total scattering cross sections.* American Journal of Physics, 2002. **70**(6): p. 620-625.
69. Li, X., L. Xie, and X. Zheng, *The comparison between the Mie theory and the Rayleigh approximation to calculate the EM scattering by partially charged sand.* Journal of Quantitative Spectroscopy and Radiative Transfer, 2012. **113**(3): p. 251-258.
70. Baffou, G., *Mie theory & Matlab code.* 2012.
71. Grehan, G. and G. Gouesbet, *Mie theory calculations: new progress, with emphasis on particle sizing.* Applied Optics, 1979. **18**(20): p. 3489-3493.
72. Brendel, R. and D. Bormann, *An infrared dielectric function model for amorphous solids.* Journal of applied physics, 1992. **71**(1): p. 1-6.
73. Nakagawara, Ryosuke & Uchida, Satoshi & Shibuya, Taiichi & Nishikawa, Hiroyuki, *Numerical Simulation of Gold Nanoparticles Dynamics in Dielectrophoretic Assembly.* IEEJ Transactions on Sensors and Micromachines, 2017. **137**: p. 107-114.

74. Mohsin, A.S. and M.B.J.I.j.o.n. Salim, *Probing the intracellular refractive index and molecular interaction of gold nanoparticles in hela cells using single particle spectroscopy.* 2018. **13**: p. 6019.
75. Tanev, S., V. Tuchin, and P. Paddon, *Light scattering effects of gold nanoparticles in cells: FDTD modeling.* Laser Physics Letters, 2006. **3**(12): p. 594.
76. Mohsin, A.S. and M.B.J.I.P.J. Salim, *Probing the plasmon coupling, quantum yield, and effects of tip geometry of gold nanoparticle using analytical models and FDTD simulation.* 2018. **10**(3): p. 1-10.
77. Kubiliūtė, Reda & Maximova, Ksenia & Lajevardipour, Alireza & Yong, Jiawey & Hartley, Jennifer & Mohsin, Asm & Blandin, Pierre & Chon, James & Sentis, Marc & Stoddart, Paul & Kabashin, Andrei & Rotomskis, Ricardas & Clayton, Andrew & Juodkazis, Saulius., *Ultra-pure, water-dispersed au nanoparticles produced by femtosecond laser ablation and fragmentation.* 2013. **8**: p. 2601.
78. A. Dhawan, S. Norton, M. Gerhold, and T. Vo-Dinh, *Comparison of FDTD numerical computations and analytical multipole expansion method for plasmonics-active nanosphere dimers.* Optics express, 2009. **17**: p. 9688-703.
79. Stephen, G., *Introduction to the Finite-Difference Time-Domain (FDTD) Method for Electromagnetics*. Introduction to the Finite-Difference Time-Domain (FDTD) Method for Electromagnetics. 2011: Morgan & Claypool. 1.
80. Kim, Deok-Soo & Heo, Jinhwa & Ahn, Sung Hyun & Han, Sang & Yun, Wan & Kim, Zee, *Real-Space Mapping of the Strongly Coupled Plasmons of Nanoparticle Dimers.* Nano Letters, 2009. **9**(10): p. 3619-3625.
81. Qin, Yaqiong & Ji, Xiaohui & Jing, Jing & Liu, Hong & Wu, Hongli & Yang, Wensheng, *Size control over spherical silver nanoparticles by ascorbic acid reduction.* Colloids and Surfaces A: Physicochemical and Engineering Aspects, 2010. **372**(1-3): p. 172-176.
82. Lumerical, F., *Solutions 8.0.* FDTD Solutions Getting Started, Release, 2013. **8**.
83. Ciracì, Cristian & Hill, Ryan & Mock, J & Urzhumov, Yaroslav & Fernández-Domínguez, Antonio & Maier, Stefan & Pendry, J & Chilkoti, Ashutosh & Smith, D, *Probing the Ultimate Limits of Plasmonic Enhancement.* Science, 2012. **337**(6098): p. 1072-1074.
84. Kumar, Vijay & Sahu, Amit & Li, Xiangping & Moshin, Abu & Gedanken, Aharon, *Refractive-index tuning of highly fluorescent carbon dots.* 2017. **9**(34): p. 28930-28938.

85. A. Taylor, P. Michaux, A. Mohsin, and J. Chon, *Electron-beam lithography of plasmonic nanorod arrays for multilayered optical storage.* 2014. **22**(11): p. 13234-13243.
86. Giannini, Cinzia & Ladisa, Massimo & Altamura, Davide & Siliqi, Dritan & Sibillano, Teresa & De Caro, Liberato, *X-ray diffraction: a powerful technique for the multiple-length-scale structural analysis of nanomaterials.* Crystals, 2016. **6**(8): p. 87.
87. Abbas, Q., *Understanding the UV-Vis Spectroscopy for Nanoparticles. J Nanomater Mol Nanotechnol 8: 3. doi: 10.4172/2324-8777.1000268 Volume 8• Issue 3• 1000268• Page 2 of 3• Result Interpretations ZnO nano particles To examine the optical properties of nanoparticles UV-Vis spectroscopy is used*. 2019, Figure.
88. Stockert, J.C. and A. Blázquez-Castro, *Fluorescence microscopy in life sciences*. 2017: Bentham Science Publishers.
89. Chamakura, Karthik & Perez-Ballestero, Rafael & Luo, Zhiping & Bashir, Sajid & Liu, Jingbo, *Comparison of bactericidal activities of silver nanoparticles with common chemical disinfectants.* Colloids and Surfaces B: biointerfaces, 2011. **84**(1): p. 88-96.
90. Kang, Hyung & Kwon, Sun-Sang & Nam, Yoon Sung & Han, Sang Hoon & Chang, Ih-Seop, *Determination of zeta potentials of polymeric nanoparticles by the conductivity variation method.* Journal of colloid and interface science, 2002. **255**(2): p. 352-355.
91. Barron, P.M.V.R.A.R., *Introduction to Atomic Absorption Spectroscopy*. 2019.
92. Kurien, S. & Sebastian, S. & Mathew, J. & George, K., *Structural and electrical properties of certain nanocrystalline aluminates.* 2005.
93. Yaseen, D. and M. Scholz, *Textile dye wastewater characteristics and constituents of synthetic effluents: a critical review.* International journal of environmental science and technology, 2019. **16**(2): p. 1193-1226.
94. Wang, Zongping & Xue, Miaomiao & Huang, Kai & Liu, Zizheng, *Textile dyeing wastewater treatment.* Advances in treating textile effluent, 2011. **5**: p. 91-116.
95. Rana, Rajender & Singh, Prashant & Kandari, Vikas & Singh, Rakesh & Dobhal, Rajendra & Gupta, Sanjay, *A review on characterization and bioremediation of pharmaceutical industries' wastewater: an Indian perspective.* Applied Water Science, 2017. **7**(1): p. 1-12.
96. *Infrared Spectroscopy Absorption Table.* 2019.

97. Coates, J., *Interpretation of infrared spectra, a practical approach.* Encyclopedia of analytical chemistry: applications, theory and instrumentation, 2006.
98. Water, a.q., *Chromium in Drinking Water*. 2016.
99. Water, a.q., *Lead in Drinking Water*. 2016.
100. Water, a.q., *Silver in Drinking Water*. 2015.
101. Sarkar, Deboleena, *Probing the interaction of a globular protein with a small fluorescent probe in the presence of silver nanoparticles: Spectroscopic characterization of its domain specific association and dissociation.* RSC Advances, 2013. **3**.

Publications:

Mehzabien Iqbal, Tasin Rahman, MD Faqrul Islam, Abu Yousha MD Abdullah, Amit Kumar Sahu and Abu S. M. Mohsin, **"Probing the optical properties of silver and gold nanoparticle and their biological applications"**, Paper Number: 389, Eighth International Conference on Nanoscience and Nanotechnology (ICONN 2020), Brisbane, Australia Sun 9 - Thu 13 February 2020, (Accepted).